E-(49-1)-3800-5
Distribution Category UC-90g

HPRF

DEVELOPMENT, TESTING AND EVALUATION OF MHD-MATERIALS

Quarterly Report

for the period July - September 1976

H. P. R. Frederikse, T. Negas and S. J. Schneider

Inorganic Materials Division
Institute for Materials Research
National Bureau of Standards
Washington, D. C. 20234

Date Published: September 30, 1976

PREPARED FOR THE UNITED STATES
ENERGY RESEARCH AND DEVELOPMENT ADMINISTRATION
Under Contract No. E(49-1)-3800

DEVELOPMENT, TESTING AND EVALUATION OF MHD-MATERIALS

Quarterly Report

for the period July - September 1976

H. P. R. Frederikse, T. Negas and S. J. Schneider

Inorganic Materials Division
Institute for Materials Research
National Bureau of Standards
Washington, D. C. 20234

Table of Contents

ABSTRACT

During the 5th Quarter there has been strong emphasis on the preparation of MHD-materials for upcoming tests, and characterization of electrode and insulator materials that have been tested recently. In the first category are the spinel materials for the U-02 test (Phase II), and the electrode/insulator assemblies (Mg-Al-Fe spinels as conductors, pure spinels as insulators) for the Reynolds test (under auspices of ANL), both to be conducted during the latter part of September. Characterization experiments (X-ray diffraction and SEM) are being performed on a variety of electrodes that were tried out in the AVCO-Mark VI generator for periods of 5 and 20 hours (with coal slag added to the fuel). Also, a new series of preheater samples, tested by Fluidyne, are being evaluated.

Calculations were made concerning the amount of various slag components in the vapor phase under conditions corresponding to those of a two-stage combustor and of a radiant boiler section (in the PERC-model of an MHD-system).

Considerable progress was made in the determination of the phase diagram of a simplified seed-slag system (K_2O-Al_2O_3-SiO_2).

Important data were obtained concerning the diffusion of potassium into alumina, and that of Fe from Mg-Al-Fe-spinel into pure Mg-Al-spinel.

In connection with cooperative programs, NBS staff members visited a number of other MHD contractors: Montana Energy Institute, Montana Tech. and Montana State University, Westinghouse, AVCO, MIT, Fluidyne and Reynolds Metals.

Objectives and Scope of Work

The overall objectives of this program are to obtain chemical and physical definition of high temperature materials which have shown promise for use in coal-fired open-cycle MHD power systems. Major problem areas in which investigations will be concentrated are:

1. Characterization of coal slag and its effects on system components and performance at prototype temperatures.

2. Development of electrode materials which provide adequate performance over extended periods of time.

3. Insulating materials which limit thermal losses and are resistant to prolonged thermal and erosion effects.

4. Preheater materials which can withstand the operating modes of separately and directly fired operation.

5. Seed recovery methods from slag which are technically and economically feasible.

6. Phase equilibria and diffusion rates of seed in slag and the corrosive action of combination on system components and materials.

7. Durability of prototype MHD sub-systems.

The program is designed to contribute to the solution of these problems by providing much needed data on candidate materials and by evaluating test samples and structures that have been subjected to real or simulated MHD conditions. The activities are grouped under six tasks:

G. Program Management Coordination (Assisting ERDA in coordination, planning and review of the various MHD-Materials Development Programs).

H. U-02 Materials Testing and Characterization (Coordination of U-02 Test Activities, Phase I).

I. Operational Design Properties (viscosity, electrical conductivity, vaporization).

J. Corrosion by Seed and Slag (phase equilibria, diffusion).

K. Materials Testing and Characterization (test coordination, pre- and post-test analysis).

L. Assessment of Steam Plant Components (corrosion resistance of metals and alloys).

Summary of Achievements - July - September 1976

(Completed Milestones - see Work Statement)

During the 5th quarter of Fiscal 1976 the following program points were accomplished in accordance with the projected milestones. In a number of cases the actual achievements differ somewhat from the plans as formulated a year ago, because of some necessary changes in work assignments and schedules, made in discussions with, and agreed upon by, staff members of the ERDA-MHD Office.

1a. Planned and prepared negotiations of the US/USSR Working Group on Testing of MHD Materials: Phase II and III.

2. Participated in reviews, planning sessions, preparation of working documents in the area of MHD-materials development. (e.g., study on Closed Cycle MHD).

4. Measured the viscosity (and electrical conductivity) of a variety of coal slags (in particular one Mid-Western and one Western coal).

20a. Determined temperatures of interfaces in one spinel-metalfelt-metal sandwich electrode under large temperature-gradient produced by a CO_2-laser.

29. Determined diffusion rates of alkali seed into various alumina samples.

39a. Assisted in the testing and pre- and post-test analysis of specimens and electrode-assemblies exposed to simulated or real MHD conditions in a variety of test rigs and generators. [U-02 (Phase II), AVCO (August test), ANL-Reynolds].

42a. Assessed the degree of hot corrosion attack on a number of steels and alloy steels designated for use in the steam superheater and reheater coils.

Task G. MATERIALS PROGRAM COORDINATION (S. J. Schneider)

Program Review and Consultation Activities

S. J. Schneider participated in the regular ERDA-MHD staff meetings and in program review meetings at AVCO, Westinghouse and Reynolds Metals (ANL U-25 Program). The conclusions and recommendations resulting from these meetings are reflected in Panel reports to ERDA or through direct consultations with ERDA staff.

NBS receives on a regular basis, MHD technical reports and proposals for review. During this period, NBS staff provided 23 such evaluations.

Arrangements and plans were also formulated relative to the various testing and characterization activities carried out between NBS and MHD-ERDA contractors (Battelle NW, Fluidyne, Westinghouse, ANL, UTSI and AVCO). These efforts relate both to the National Program and to the US-USSR Cooperative Program. Special emphasis is placed on the transfer of information and data to participating groups so that maximum impact to individual development programs can be gained.

US-USSR Cooperative Program (Materials)

Major emphasis this period was focused on the coordination of the various activities required to effect the Phase II U-02 in September 1976. The test modules (anode and cathode walls) were delivered on schedule by Westinghouse in August 1976. The test plan, worked out by Westinghouse and NBS and approved by the USSR, forms the basis for a 100 hr. endurance test under MHD (U-02 conditions). The results from this test will provide important information necessary for the selection of the electrode system of the U-25 channel being developed through ANL management.

In preparation for the forthcoming October Working Group meeting in Moscow, a tentative program for the U-25 high field loop has been formulated. Also, work continues on the materials section of the Joint US-USSR MHD Status Report. In this context, the USSR input has been reviewed and a suggested revision by USSR was requested.

Closed Cycle Program Assesment

In cooperation with RAND Corporation, NBS has been actively engaged in the status and assessment of closed cycle MHD technology. S. J. Schneider served as chairman of the June 28-July 2, 1975 ERDA-RAND Conference on Closed Cycle MHD and additionally is providing input on a continuing basis to the preparation of RAND assessment documents.

Task H. U-02 Materials Testing and Characterization (Phase I) (W.R. Hosler)

Final Report U-02 Test (Phase I)

The Soviet contributions to the report have now been incorporated. The report will be submitted to the US/USSR Steering Committee for approval in October.

Task H was completed as of June 30, 1976.

Task I. OPERATIONAL DESIGN PROPERTIES

a. VISCOSITY OF COAL SLAGS (W. Capps and D. A. Kauffman, Inorganic Glass Section)

Introduction

In order to better coordinate the efforts of the many MHD contractors, a decision was made to "standardize" on a typical midwestern and a typical western coal. These are Illinois #6 coal and Montana Rosebud coals. This will reduce the compositional range of coal slags to be encountered and will facilitate comparisions of data, etc. Caution must be used, however, because even these two coals cover a fairly wide compositional range and two samples of the same coal can be quite different in composition.

Slag Preparation and Viscosity Measurement

Viscosities were determined for several real coal slags and of several synthetic slags made to resemble slags whose analyses were available.

1) Melt No. K615 is a synthetic slag whose composition was made to resemble the Illinois #6 slag analysis from the NASA ECAS specifications. One deviation from this was the intentional omission of SO_3. The viscosity-temperature relationship is shown in Fig. 1.

2) Some flyash from the Bureau of Mines PERC combustor resulting from combusion of Illinois #6 coal was melted. Viscosities are shown in Fig. 1. This is K769.

3) A synthetic slag was made from an average composition from five analyses of Illinois #6 coal slags listed in the Selvig and Gibson report. K748 has no sulfur. Viscosity data is shown in Fig. 1 and is nearly identical to data for K615 above.

4) A synthetic slag was made identical to K748 above with 5% SO_3 added. This is K749 and is also shown in Fig. 1. The SO_3 lowers the viscosity about 9% over the temperature range shown. Both K748 and K749 have lower viscosities than the real ash (K769).

5) Some bottom ash from Montana Rosebud coal was obtained from a commercial power plant. Several independent determinations of viscosity were made and are shown in Fig. 2 as melts K603 and K624. Results are quite similar.

6) A synthetic Rosebud slag was made from the NASA ECAS specifications and contained a very high sulfur content. This is K612; the viscosity is quite different from the bottom ash as shown in Fig. 2.

7) Another synthetic slag was made of the same proportions of the oxides as in K612 with the SO_3 left out in order to see what role the SO_3 might play. This is K620. Its viscosity is higher than K612 showing that here too the SO_3 lowers the viscosity. See Fig. 2. However, even without the SO_3 the viscosity is much lower than the real bottom ash (K603 or K624).

8) Flyash from the same Montana power plant as K603 and K624 formed by burning Rosebud coal was measured. This proved very difficult as the melt out-gassed for a long period at 1400 C causing a foamy crust to form which was too viscous to allow the bubbles to escape. At 1600 C the crust was fluid enough to permit the foam to collapse and allow the melt to clear of bubbles. The viscosity is shown in Fig. 2 and is similar to the bottom ash from the same coal.

PLANS

1. Measure viscosity of a MHD channel slag from the University of Tennessee Space Institute from Illinois #6 coal.

2. Make a synthetic slag having the composition of the Russian Krushnitz coal slag. Measure viscosity.

3. Try to identify cause of excessive bubbling of Montana Rosebud power plant flyash.

4. Continue study of role of SO_3 in determining viscosity.

Table 1. Coal Slag Composition

Illinois #6
(Weights percents)

	SiO_2	Al_2O_3	Fe_2O_3	CaO	MgO	TiO_2	P_2O	Na_2O K_2O	SO_3
ECAS SPECS	46.6	19.3	20.8	7.7	0.9	0.8	0.2	1.9	24
Average Selvig and Gibson	48.4	21.5	21.5	7.5	1.1	--	--	--	-
NBS K615	47.6	19.7	20.5	7.9	0.9	0.8	--	2.6	--
PERC Flyash K769	45.7	16.3	16.8	9.5	1.1	1.1	--	2.9	6.5
K748	48.4	21.5	21.5	7.5	1.1	--	--	--	--
K749	46.0	20.4	20.4	7.2	1.0	--	--	--	5.0
			Montana Rosebud						
ECAS SPECS	22.1	15.5	6.4	18.9	6.6	1.2	0.1	1.4	26.2
K612	22.4	15.7	6.3	19.1	6.7	1.2	--	1.4	27.3
K620	30.7	21.5	8.9	26.2	9.2	1.7	--	1.9	--
Bottomash K603 Flyash K779*	55.0	19.5	5.4	10.0	4.0	0.8	0.12	0.66	4.2

*Analysis furnished by Montana State University.

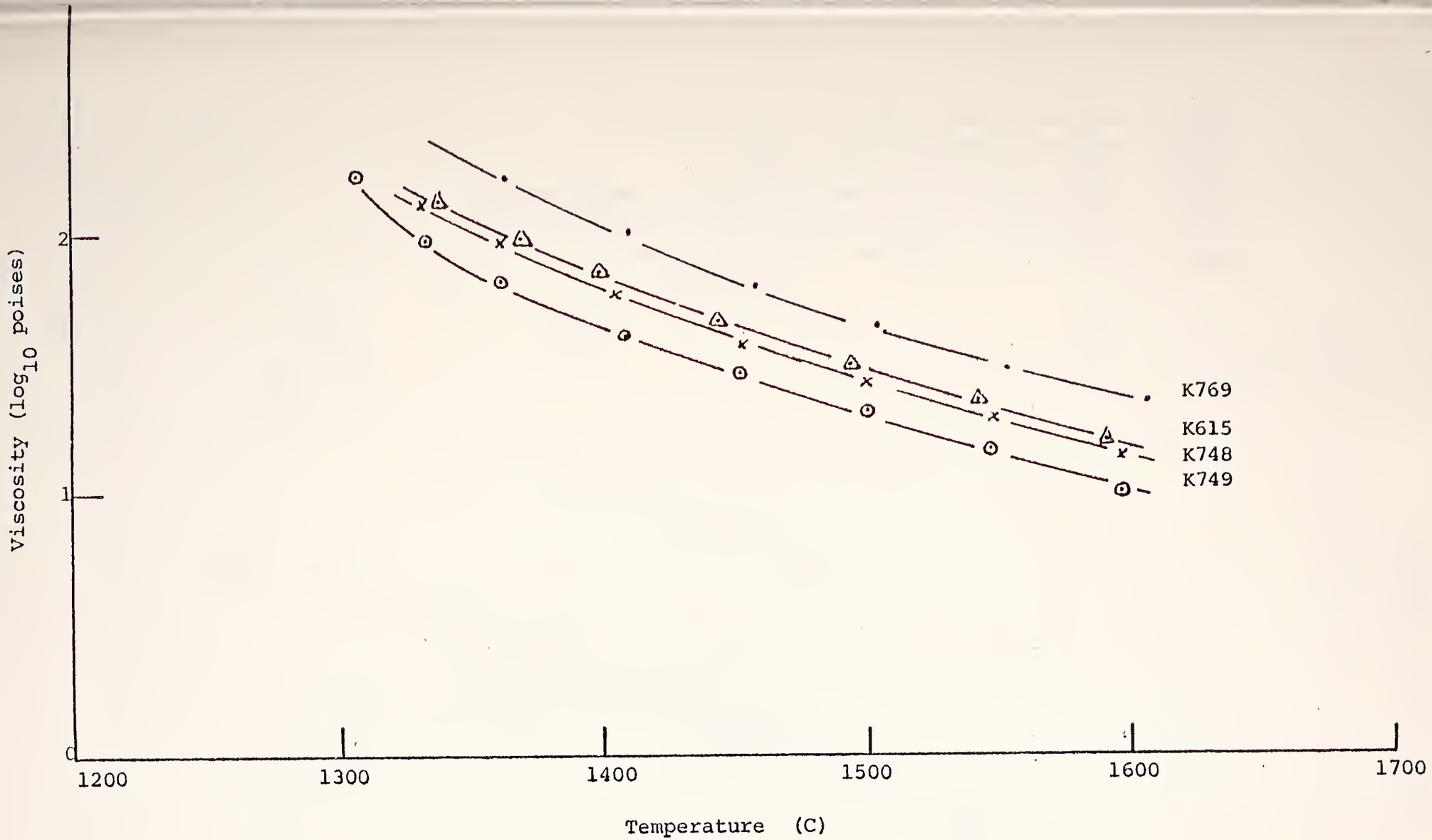

Figure 1. Viscosity of Illinois #6 Coal Slags

K769 Combustor Flyash, Pittsburgh Energy Research Center, Bureau of Mines.
K615 NASA ECAS Specifications.
K748 Average Composition from Selvig & Gibson of 5 Ill. #6 coals (No SO_3).
K749 Average Composition from Selvig & Gibson of 5 Ill. #6 coals (5% SO_3).

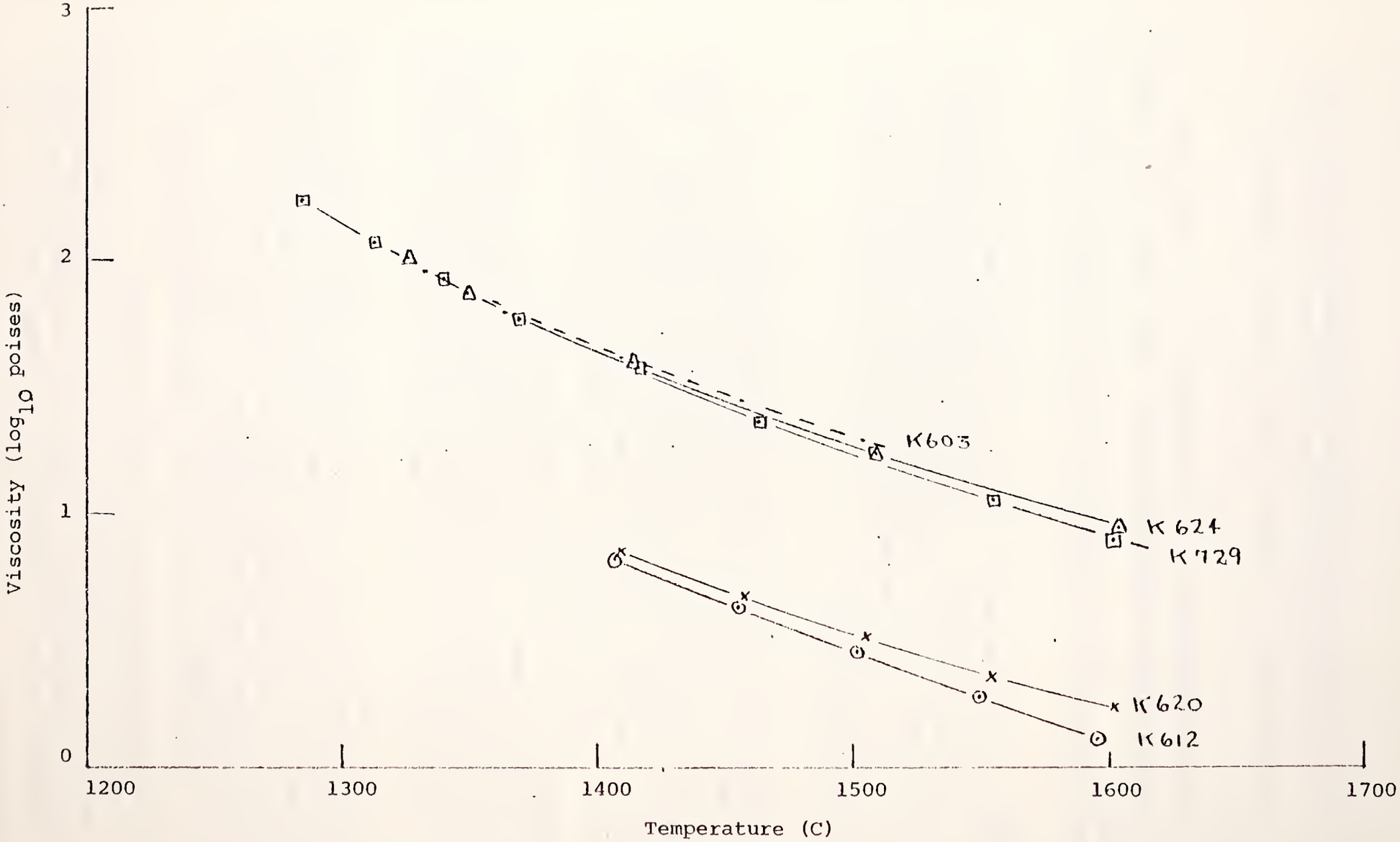

Figure 2. Viscosity of Montana Rosebud Coal Slags.

K603 Bottom Ash from Montana Power Plant, (Sample No. 1).
K624 Bottom Ash from Montana Power Plant (Sample No. 2).
K729 Flyash from Montana Power Plant.
K620 NASA ECAS Specifications (with no SO_3.
K612 NASA ECAS Specifications (with 27.3% SO_3).

b. Electrical Conductivity (A.J. Armstrong, W.R. Hosler, H.P.R. Frederikse)

During this reporting period the electrical conductivities of two representative coal slags were investigated. Conductivity measurements were also performed on 5 electrode materials that will be tested in the U-02 MHD facility in September. In addition, extensive changes were made in the cooling system on the ASTRO high temperature-controlled atmosphere furnace.

Coal Slag. The two coal slags whose electrical conductivities have been measured in air are Montana Rosebud and Illinois #6. (Figs. 3 and 4). The Montana Rosebud slag is from power plant bottom ash obtained via Mr, W. Capps of NBS. The Illinois #6 slag was removed from the generator walls of the UTSI MHD facility and was obtained from Dr. L. Crawford of UTSI. The conductivity of the Rosebud slag below 1150 °C is much lower than that of other coal slags; in that range the conductivity falls on the very edge of the "allowable window" as calculated by R. J. Rosa.[1]

U-02 Materials. The electrical conductivities of the two NBS spinel electrode materials (both were $3MgAl_2O_3:1Fe_3O_4$) are shown in Figs. 5 and 6. The results agree closely with those measured previously on this same material and reported in our previous quarterly report. It should be realized that the magnitude of the conductivity depends somewhat on the structural properties (porosity, grain size, etc.) determined by the particular fabrication method.

Of the three other U-02 electrode materials investigated, two were $LaCrO_3$ with approximately 5% MgO added. (Westinghouse and General Refractories). Both samples evidenced somewhat higher electrical conductivity (Figs. 7 and 8) than that reported for pure $LaCrO_3$ by Grabner, Hosler and Frederikse.[2] The third electrode material, 75% hercynite + 25% magnetite, (developed by MIT) showed a marked change in electrical conductivity in air below 1300 °C (Fig. 9). As this was not seen in 10^{-3} and 10^{-6} oxygen partial pressures obviously oxidation and reduction has a lot to do with this abrupt change.

Watercooling for the ASTRO Furnace

During the past half year problems have arisen with the cooling coils of the ASTRO-furnace. Boiler scale has built-up on the hot surfaces in contact with the hard cooling water. After considering various deflocculants or filters it was decided to replace the water-cooling system with a closed one using distilled water and a heat exchanger. In this heat exchanger the continuously circulating supply of distilled water is cooled by chilled water of the central laboratory system.

Future Work:

1. The electrical conductivity of spinels with various amounts of Fe_3O_4 will be investigated.
2. The conductivities of other eastern and western coal slags will be measured.
3. The effect of specific admixtures on the conductivity of coal slag will be explored.

---

[1] R. J. Rosa, AVCO Monthly Report of Office of Coal Research, January 1975.

[2] L. H. Grabner, W. R. Hosler and H. P. R. Frederikse, Proc. of the 14th Symp. on Engineering Aspects of MHD Power Generation, Tullahoma, TN, April 1975.

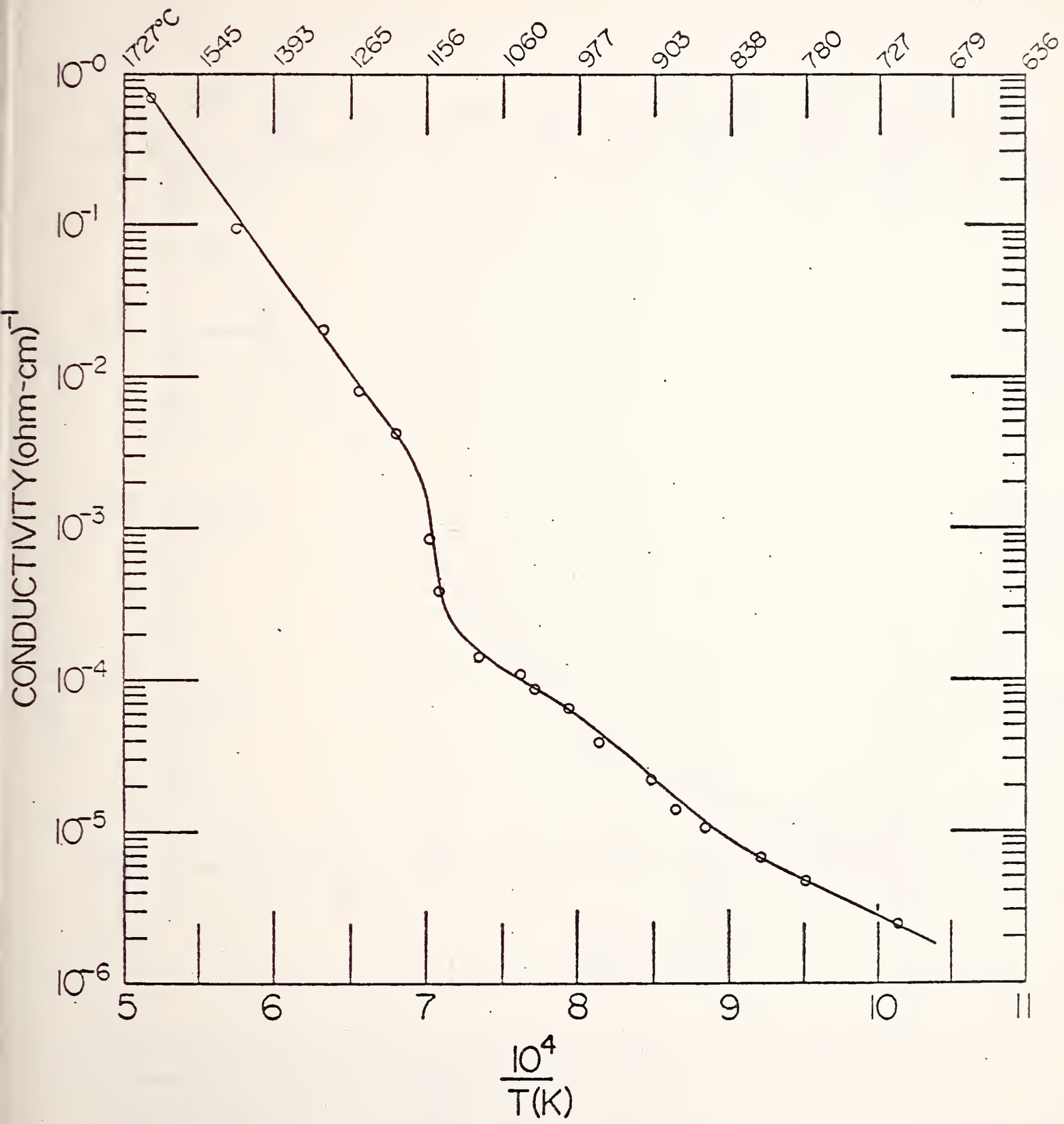

Fig. 3. Electrical conductivity of coal slag (Montana Rosebud) as a function of temperature measured in air.

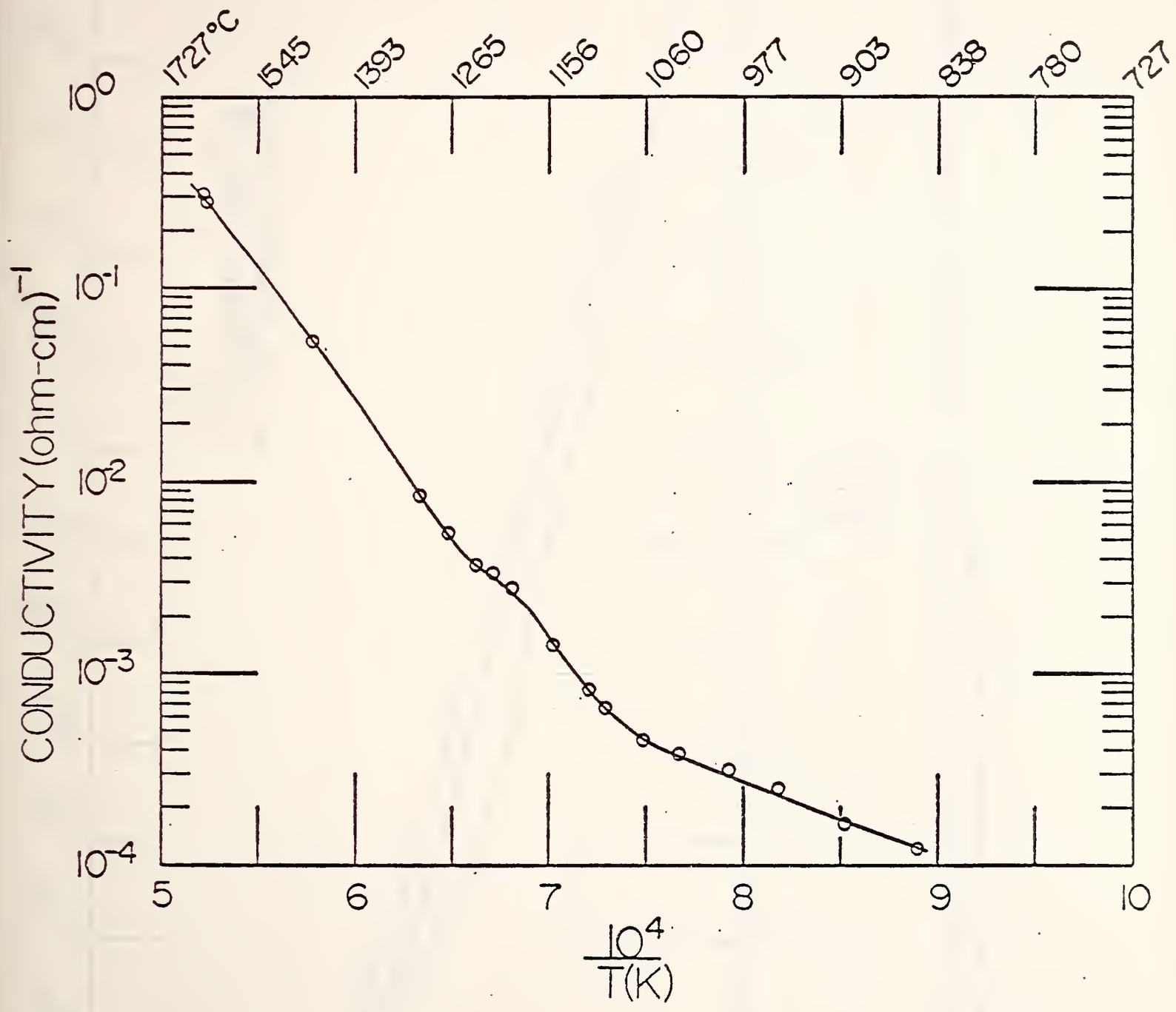

Fig. 4. Electrical conductivity of coal slag (Illinois #6) as a function of temperature measured in air.

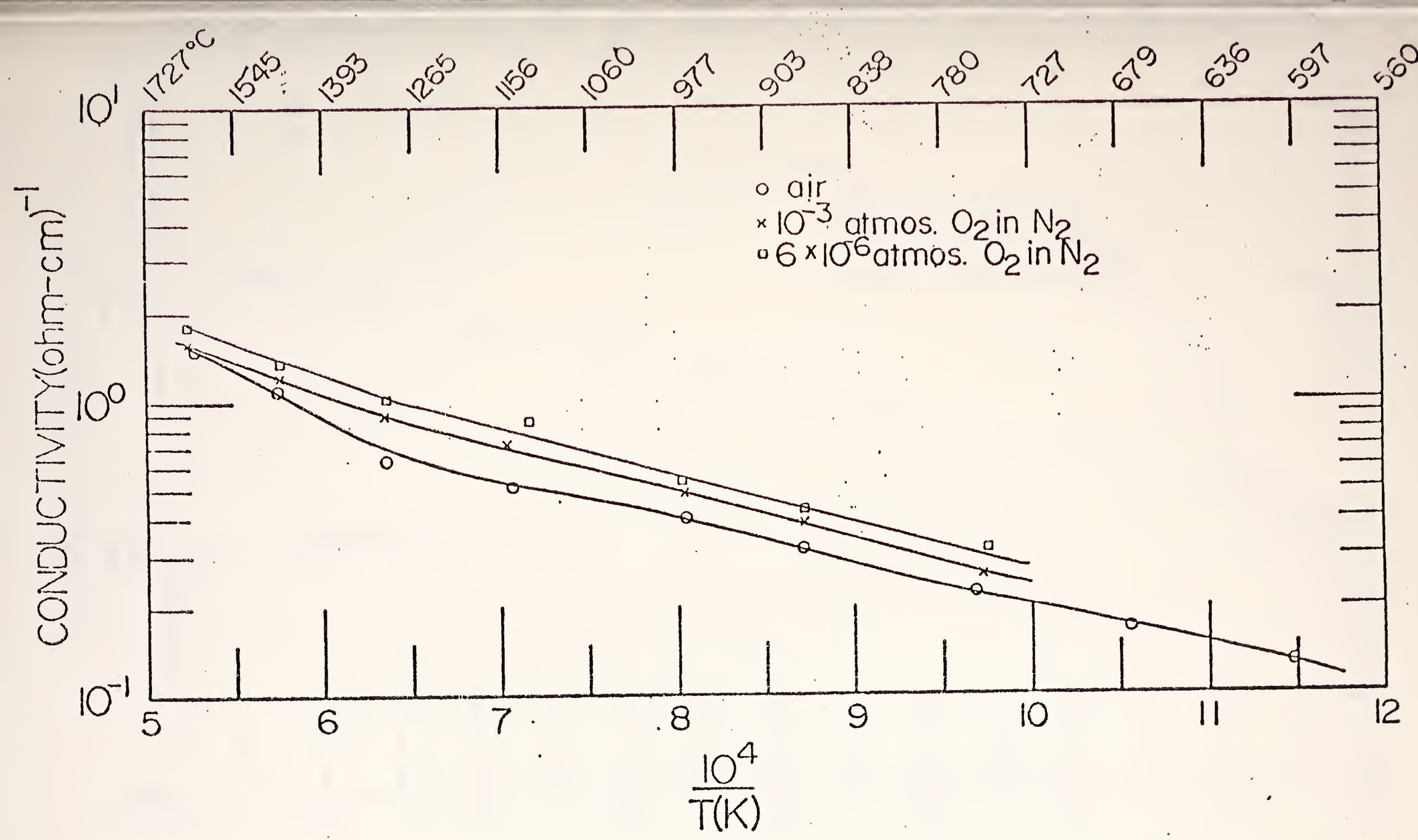

Fig. 5. Electrical conductivity of porous spinel 75 $MgAl_2O_4$ - 25 Fe_3O_4 as a function of temperature at several partial pressures of oxygen. (BNW).

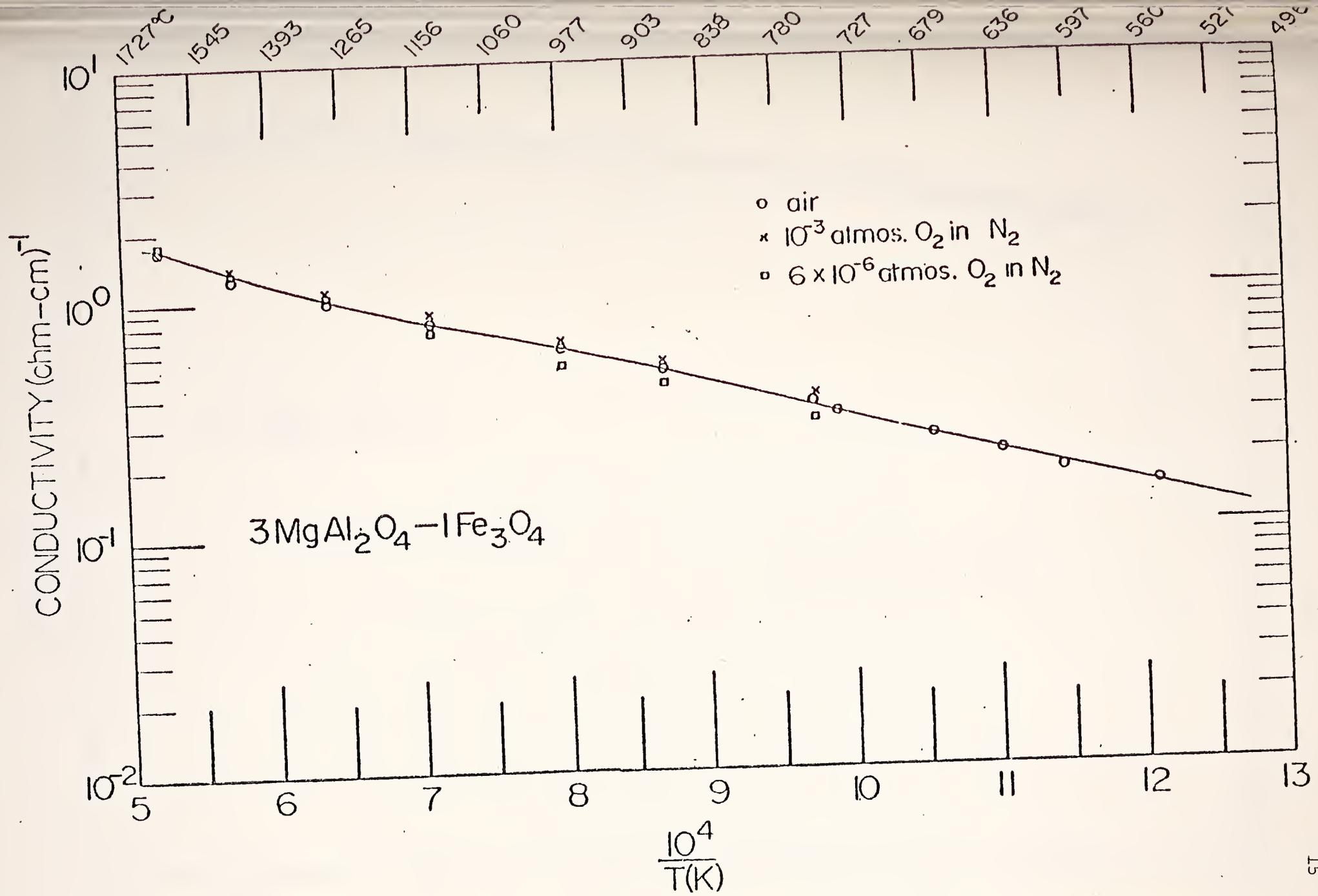

Figure 6. Electrical conductivity of sintered spinel electrode material at elevated temperatures and various oxygen partial pressures.

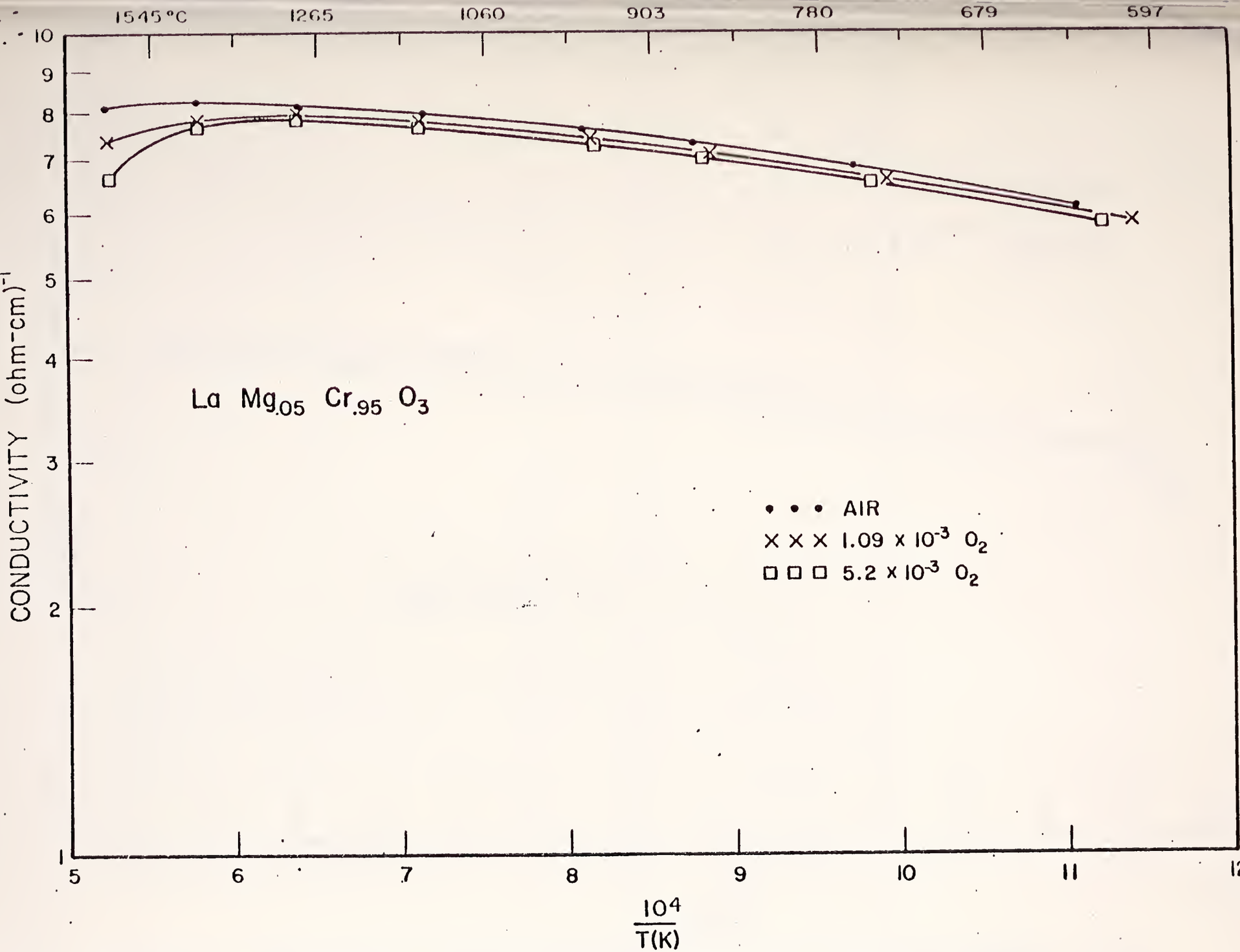

Fig. 7. Electrical conductivity of $LaCrO_3$:Mg (G.R.) as a function of temperature as pressure.

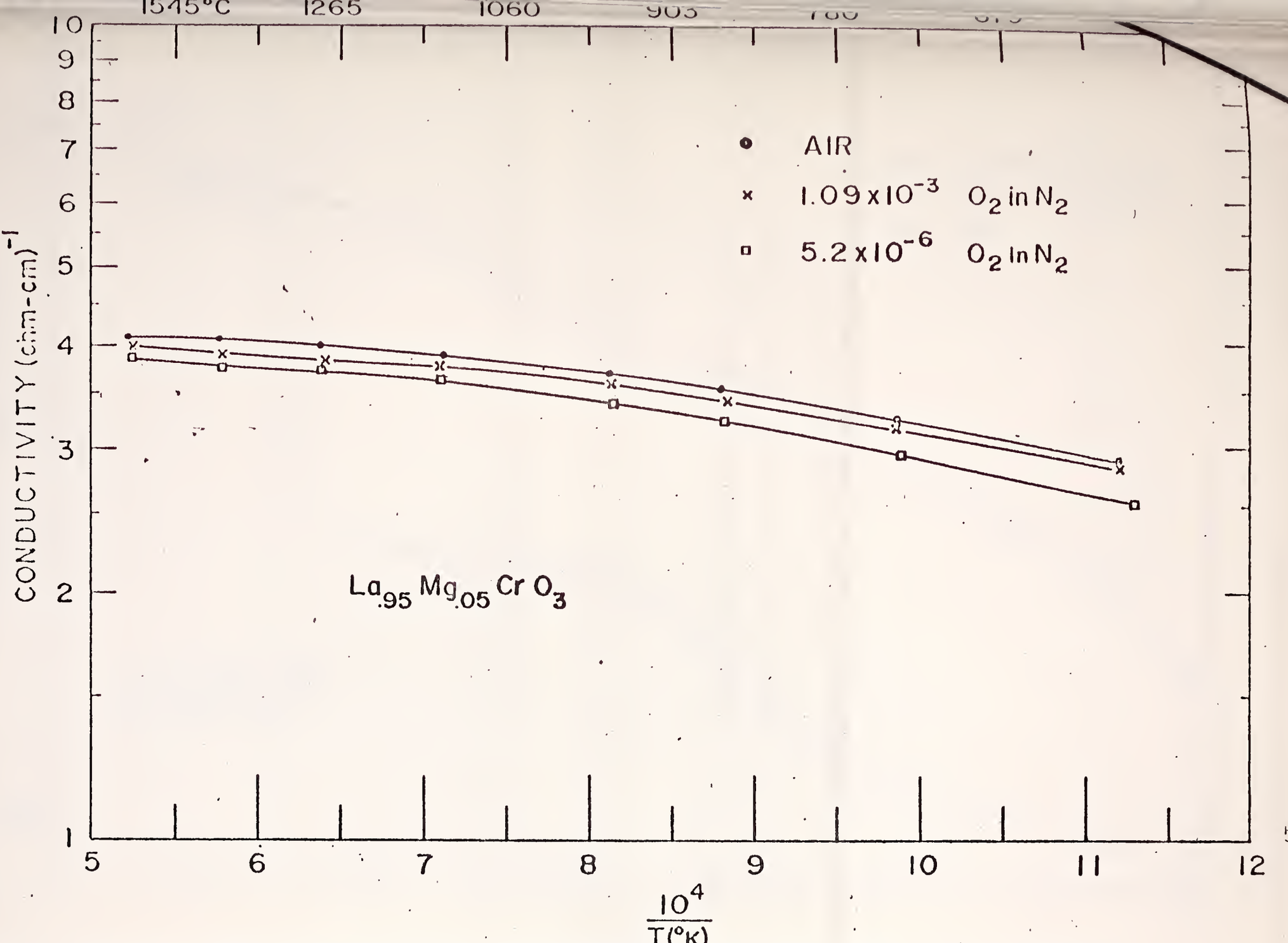

Fig. 8. Electrical conductivity of $LaCrO_3$:Mg (Westinghouse) as a function of temperature and pressure.

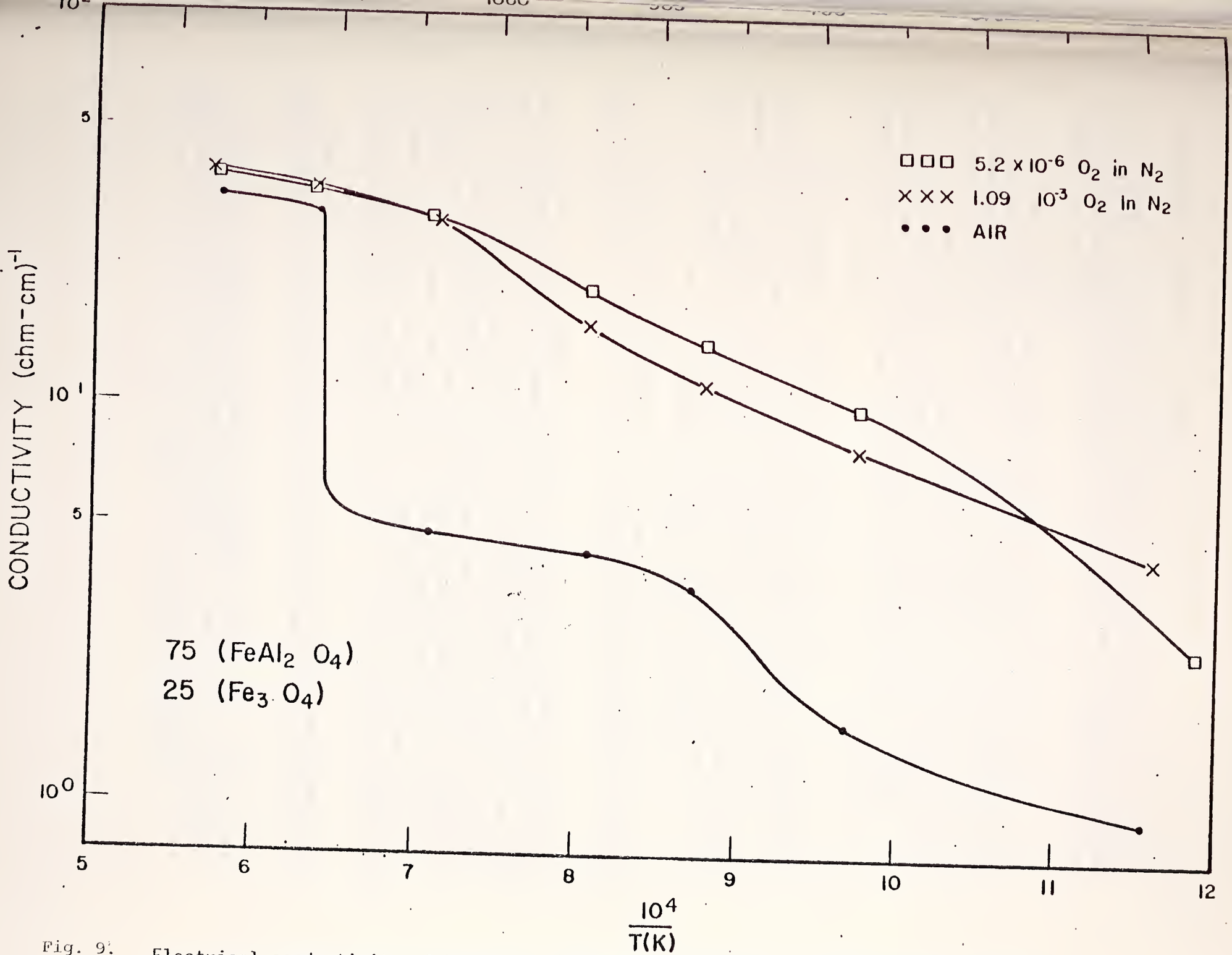

Fig. 9. Electrical conductivity of hercynite (LASL) as a function of temperature at several partial pressures of oxygen.

c. Vaporization Studies (E. R. Plante)

During this quarter it was requested that NBS analyze the problems of combustor slag rejection, slag fractionation and the general problems of slag composition as a function of wall position in an MHD channel and downstream components.

At the present time, a difference of opinion exists concerning the optimum value of ash carry over. Some consider that the liquified coal ash components can serve as a continually renewable protective layer for the electrode structure of an MHD channel which will protect the electrode structure from erosion, corrosion and destructive arcs while not appreciably degrading channel performance. As a matter of fact, coal slag is considered as a potential channel replenishment material. If true, insufficient slag carryover could lead to bare spots and degradation or electrode structures.

Others however, believe that generator performance will of necessity be impaired by the presence of liquid ash because of short circuiting of electrode structures. In addition, the problem of seed recovery is expected to be more difficult if the seed has the opportunity to react with large amounts of coal ash. Finally, the amount of dust and fly ash in a system with large percentages of ash carryover are seen as difficulties leading to possible plugging problems for air preheaters.

In view of these problems, it has generally been considered desirable if possible to design and operate a combustor which is capable of rejecting 90% of the ash.

A review of MHD combustor designs was presented by Henry, Kurtzrock and Bienstock (1) who advocate the idea that high ash rejection is desirable. As a limitation on ash rejection in a one stage combustor, they state that "Equilibrium calculations (with the technique of Spencer, 1973) of combustion of coal (a Pittsburgh seam bituminous coal) at a pressure of eight atmospheres with about 90% of stoichiometric air preheated to a temperature of 1280K with 6% heat loss predict a plasma temperature of about 2660K. At these conditions, more than 25% of the coal ash is predicted to be vaporized. This puts an apparent upper limit on slag rejection capabilities of single-stage MHD combustors of 75%."

The purpose of this discussion is to outline some of the concepts and thermodynamic reasoning that can be called into play in such design considerations.

The actual combustion process is extremely complicated. The rate of vaporization of slag particles may be limited by the rate of diffusion of vapor away from the particle, or by the rate at which heat flows to the particle. In addition, it will depend on the particle composition.

At any specified temperature, pressure, and oxygen/fuel ratio one can estimate the fraction of slag that would be in equilibrium with a condensed slag phase if some assumptions concerning the activity of slag components in the condensed phase are made. Variations in the basic assumptions are possible. For example, the ash components in the coal feed stock are probably not homogeneous so that more ash components might be present in the vapor phase than would be if establishment of equilibrium with respect to a hypothetical ideal solution were achieved. In addition, ash components can be transported to the vapor phase via formation of a number of different types of reactions and equilibrium with respect to each reaction may not necessarily be established.

The metals from principal ash components can be carried in the vapor phase as a variety of species as indicated in Table 1.

These species were assumed to be formed in the calculations.

Table 1

Ash Component	Vapor Species
SiO_2	SiO, SiO_2, Si
MgO	Mg, MgO, MgOH, $Mg(OH)_2$
CaO	CaO, Ca, CaOh, $Ca(OH)_2$
FeO	Fe, FeO, $Fe(OH)_2$
Al_2O_3	Al, AlO, AlO_2, AlOOH, Al_2O, $Al(OH)_2$, AlOH, Al_2O_2

For purposes of this report and following the method adopted by Spencer and Orning (2), we assume that the slag components are present in an ideal liquid solution and that equilibrium is established with respect to all reactions. Having calculated the amount of slag in the vapor phase it is assumed that most of the slag remaining in the liquid phase is effectively removed to the cooled sidewalls by the swirl action of the combustor.

Thermodynamic data used in our calculation are from JANAF (3), using tables furnished through December 31, 1975 except for data for $Al(OH)_2$ which was taken from Jensen and Jones (4). The data for $Al(OH)_2$ was obtained by flame photometric spectroscopy and has not been confirmed by other laboratories. For example, Farber et al (5) were unable to detect the $Al(OH)_2$ molecule by mass spectrometric observations of Al in H_2/O_2 flames where it presumably would be a major Al-bearing species. Rejection of $Al(OH)_2$ as a possible Al-bearing species would decrease the volatility of Al_2O_3 significantly. It would not however have a significant effect on the conclusions drawn from this calculation.

The variation in the amount of vaporization of each slag component depends on the relative importance of each of the vapor species. The greatest change in the amount of vaporization as the O/F ratio changes occurs for SiO_2, followed by FeO and MgO while the effects are relatively small for CaO and Al_2O_3. This is due to the relatively more important transport of slag components by SiO, Fe, and Mg gases while a significant amount of transport of CaO and Al_2O_3 is due to formation of hydroxide species.

Whether or not there is significant fractionation of the coal ash will depend to some extent on the temperature at which slag separation in the first stage of the combustor takes place and the fraction of slag carried as particulate matter. The amount of SiO_2, FeO, and MgO transported to the vapor phase depends much more strongly on temperature than does the transport of CaO and Al_2O_3. Thus, if the separation takes place at a relatively low temperature, such as 2300K, fractionation effects will not be very great. Any fractionation that takes place because of the vaporization processes will tend to be reduced because of carryover of particulate material.

The results obtained here generally confirm the concept that large slag rejection can be achieved in a two stage combustor provided that a high percentage of particulate matter can be removed by the swirl motion of the combustor. Some typical values for ash rejection based on a Montana Colstrip coal are shown in Table 2. For this calculation the Montana Colstrip coal composition is approximated on a molar basis as: C=1.0, H_2=.393, N_2=.0046, H_2O=.0207, O_2=.0815, SiO_2=.0195815, Al_2O_3=.00582960, CaO=.00590433, FeO=.00388640 and MgO=.00272795. This calculation assumed that preheated air having a nominal N_2/O_2 molar ratio of four of sufficient quantity to give an overall O/F ratio of 0.6 or 1.0 was burned at a total pressure of 10 atm or 1 atm to achieve a final temperature of 2300K.

Table 2

Amount of Slag in Vapor Phase at Equilibrium at 2300K

	Percent Vaporized	
Component	P=10,O/F=.6	P=1,O/F=1.0
SiO_2	4.3	1.8
FeO	4.0	4.1
Al_2O_3	2.0	.66
CaO	1.7	2.8
MgO	2.8	2.1
Vaporized	3.3 (wgt)	1.9 (wgt)

The conditions P=10 atm, O/F=0.6, T=2300K are approximately what one would expect at the exit of the first stage of a two stage combustor while the conditions for P=1atm, O/F=1.0, T=2300K are approximately what would be found in the diffuser-radiant boiler section of an MHD system. Since the walls of the system will in general be below 2300K, nucleation and growth of liquid slag particulates in the boundary layer region of the channel can take place and slag will be transported to the wall surfaces. Because of the relatively long life of slag on the channel walls as compared to slag particulate matter in the core flow, the possibility that significant variation in composition of channel slag can take place seems remote. Rather, channel slag is likely to approach a "steady state" composition which will shift slowly in composition as variations in the input coal ash composition take place.

Future Work:

1. Vaporization measurements on selected K_2O-containing slag will be resumed.

2. Additional calculations of slag vaporization problems will be carried out if necessary.

References:

1. J. M. Henry, R. C. Kurtzrock and D. Bienstock, Proc. NSF-OCR Engineering Workshop on MHD Materials, MIT, Nov. (1974).

2. F. E. Spencer, Jr., and A. A. Orning, U.S.B.M. R.I 7786 (1973).

3. JANAF Thermochemical Tables, Dow Chemical Co., Midland, Mich.

4. D. E. Jensen and G. A. Jones, J.C.S. Faraday 68, 259 (1968).

5. M. Farber, R. D. Srivastava, M. A. Frisch and S. P. Harris, Faraday Symposium 8, High Temperature Studies in Chemistry, London, (1973).

Task J. Corrosion and Diffusion

a. Seed-Slag Interaction (L. P. Cook, C. L. McDaniel, T. Negas)

Phase Equilibria in the System K_2O-Fe_2O_3-Al_2O_3-SiO_2

The Join $KAlO_2$-$KAlSiO_4$. Experiments using $KAlO_2$-SiO_2 mixtures continued. The rapidity with which phase equilibria data can be gathered is limited by the sluggishness of subsolidus reactions; for example, compositions heated at 1400 °C must be reground and reheated four or five times before no further changes in the x-ray powder patterns occur. A similar number of heat treatments appears to be necessary at 1600 °C. Surface energy and strain energy may provide most of the driving force for reaction, since compositional differences of reacting phases are small in the vicinity of $(KAlO_2)_{50}(SiO_2)_{50}$. Metastable equilibria also appear to be important. Phenomena such as metastable melting and metastable persistance of low temperature solid solutions upon heating have been observed.

Crystalline phases occurring along the join $KAlO_2$-$KAlSiO_4$ are: hexagonal $KAlSiO_4$ (occurs in several polymorphs; reported by other investigators at low temperatures but not encountered in this study); "low temperature" orthorhombic $KAlSiO_4$, "high-temperature" orthorhombic $KAlSiO_4$, tetragonal $K_{1+x}Al_{1+x}Si_{1-x}O_4$, cubic $K_{1-x}Al_{1-x}Si_xO_2$, and non-cubic $KAlO_2$. Crystallographic properties of these phases were summarized in the previous quarterly report (Ref. 1). Tentative limits of solid solution at 1400 °C and 1600 °C can be set on the basis of experimental data accumulated to date. At 1400 °C, "low-temperature" orthorhombic $KAlSiO_4$ ranges from ∿48.5 to ∿51.5 mole % $KAlO_2$, tetragonal $K_{1+x}Al_{1+x}Si_{1-x}O_4$ ranges ∿56.5 to ∿58.5 mole % $KAlO_2$, and cubic $K_{1-x}Al_{1-x}Si_xO_2$ solid solution extends to ∿20 mole % SiO_2. At 1600 °C, "high-temperature" orthorhombic $KAlSiO_4$ ranges from ∿47.5 to ∿51.5 mole % $KAlO_2$, tetragonal $K_{1+x}Al_{1+x}Si_{1-x}O_4$ ranges from ∿55 to ∿56.5 mole % $KAlO_2$, and cubic $K_{1-x}Al_{1-x}Si_xO_2$ solid solutions extend to ∿25 mole % SiO_2. Experiments thus far have not succeeded in dissolving more than 25 mole % SiO_2 in the cubic solid solution. The extent of solid solutions at temperatures below 1400 °C are difficult to measure, and it may be necessary to resort to hydrothermal equilibration if phase equilibria data at temperatures below 1100 °C are needed. Metastable "low-temperature" orthorhombic $KAlSiO_4$ solid solutions containing up to ∿56 mole % $KAlO_2$ exist briefly at 1400 °C before decomposing, and it is probable that the solid solution field of this phase widens in the direction of $KAlO_2$ at temperatures below 1400 °C.

The nature of the phase transition occurring in orthorhombic $KAlSiO_4$ at 1400-1450 °C is uncertain, hence, the designation "high-temperature" and "low-temperature". Data accumulated thus far suggest it is reversible, but that a compositional effect may be involved. If it is reversible, the

fact that increasing temperature favors a phase with doubled unit cell requires an explanation - conclusive determination of the phase diagram in the vicinity of $KAlSiO_4$ will require a thorough understanding of the structure of the phases involved.

Liquidus temperatures in the vicinity of $KAlSiO_4$ have proved to be higher than suggested by previous work (Ref. 2). Our experiments to date suggest a liquidus temperature at ~1850 °C for composition $(KAlO_2)_{50}(SiO_2)_{50}$. The temperature at which melting begins for compositions intermediate between cubic and tetragonal solid solutions appears to be in the range 1850 - 1870 °C. With the experimental set-up employed (sealed $Pt_{60}Rh_{40}$ capsules heated inductively in an iridium crucible), quenching was difficult, and a combination of data from x-ray diffraction, light microscopy and SEM examination has been employed. The latter technique (Figs. 10a,b and 11a,b) has proved to be especially useful in this regard. Whereas $KAlSiO_4$ melts have been cooled to a glass, melts richer in $KAlO_2$ appear to crystallize more readily.

Experiments in the Ternary System K_2O-Al_2O_3-SiO_2. Results of TGA and mass spectrometric vaporization studies on crystalline $KAlSiO_4$ were given in a previous quarterly report. (Ref. 3). Two unexplained features were noted: 1) The failure of the three phase mixture $KAlSiO_4$-"β-Alumina"-$KAlSi_2O_6$ to buffer P_K and, 2) the fact that the vacuum decomposition reaction of $KAlSiO_4$ involves $KAlSi_2O_6$ and "β-Alumina", rather than $KAlSi_2O_6$ and Al_2O_3, as the equilibrium diagram (Ref. 2) suggests should be the case. 1) could in part be explained by the presence of local concentration gradients in phases of variable composition (both $KAlSiO_4$ and "β-Alumina"). To check the possibility that 2) indicated an error in the published equilibrium diagram, subsolidus experiments were conducted on mixtures of 33 mole % $KAlSiO_4$/67 mole % α-Al_2O_3 at 1500 °C for approximately two weeks, with periodic grinding. Results showed formation of a small amount of $KAlSi_2O_6$ and "β-Al_2O_3" initially, which disappeared with subsequent heat treatment. Further changes in the x-ray powder patterns with continued heat treatments showed only annealing of $KAlSiO_4$ and α-Al_2O_3. These results are interpreted as verification of a tie line between $KAlSiO_4$ and Al_2O_3 at the expense of a tie line between "β-Al_2O_3" and $KAlSi_2O_6$. The decomposition of $KAlSiO_4$ reported above may represent a metastable phenomenon. The topological relationship of this decomposition reaction to the more stable decomposition reaction, which could be prevented by the kinetics of Al_2O_3 nucleation and growth, is portrayed schematically in Figure 12.

The Join $KFeO_2$-SiO_2. A study of the subsolidus relationships on the $KFeO_2$-SiO_2 join has been initiated. A series of nine $KFeO_2/SiO_2$ mixtures have been prepared under dry-environment conditions. While $KFeO_2$ is extremely hygroscopic, reacted mixture of $KFeO_2/SiO_2$ are not. Preliminary experiments indicate at least four subsolidus phases exist in the system. The low temperature form of $KFeSiO_4$ was indexed with a hexagonal cell, a = 5.28Å and c = 8.82Å. This compound has a phase transition at 945 °C, forming a crystalline phase which at the present has undetermined symmetry. Complete melting was observed at 1100 °C for compositions rich in SiO_2 and 1400 °C in the silica-poor region. Future experiments will concentrate on the crystal chemistry and the liquidus temperatures of the crystalline phases.

Container Materials for High Temperature Liquidus Studies. Special techniques for liquidus studies along the join $KAlO_2$-$KAlSiO_4$ are clearly necessary in view of the facts that temperatures above 1900 °C are required, noble metal capsules are not capable of reaching these limits, and encapsulation is essential to prevent "K_2O" loss. Use of sealed refractory metal tubes (e.g., Ta) in an evacuated high temperature graphite furnace seems to be the best possibility. Calculation of one possible capsule corrosion mechanism at 2000 °C has been carried out:

$$5\ SiO_2(\ell) + 2\ Ta(s) \rightarrow 5\ SiO(g) + Ta_2O_5(\ell)$$

Corrosion according to this mechanism should not be serious. However, reaction with $KAlO_2$-containing mixtures is more difficult to estimate, and an experimental evaluation will be necessary.

Capsule reaction with iron in the $KFeO_2$-$KFeSiO_4$ system is severe, but it is hoped that use of $Ag_{30}Pd_{70}$ capsules will eliminate this problem at elevated temperatures.

Implications for MHD Materials Research. Potassium aluminosilicates are highly refractory materials, and in the presence of a K-rich vapor phase can be expected to be stable in the presence of silicate slags up to temperatures approaching their melting points. The implication of this is that slag accumulating in the MHD channel under operating conditions may contain crystalline $KAlSiO_4$ and related phases. For iron-rich slags, the chances of their occurrence is diminished, however. The effect of a crystal/liquid mixture on such properties as electrical conductivity and viscosity may have to be examined.

Attention should be called to the possibility of using $KAlO_2$-SiO_2 phase equilibria to deduce temperature gradients during MHD runs. Reactions in this system (especially reactions of the homogeneous type) are sluggish enough to prevent back-reaction, provided shut-down is not exceptionally slow. Once the equilibrium diagram has been determined, possibilities should be apparent. Likely candidates are the hexagonal $\rightleftarrows$ orthorhombic transition and the "low-temperature" orthorhombic $\rightarrow$ "high-temperature" orthorhombic transition.

Determination of phase relations in the systems $KAlO_2$-$KAlSiO_4$ and $KFeO_2$-$KFeSiO_4$ should provide a starting point for the systematic extension of seed/slag interaction studies to cover other systems. In particular, it is suggested that the relative effects of increasing mole % CaO, MgO and FeO on $KAlSiO_4$-rich compositions can be seen by looking at the systems CaO-$KAlO_2$-SiO_2, MgO-$KAlO_2$-SiO_2 and FeO-$KAlO_2$-SiO_2, respectively. Preliminary studies in the system CaO-$KAlO_2$-SiO_2 (Ref. 4) have shown that it is ternary and that increase in mole fraction CaO causes a significant increase in a_{K_2O} for compositions with a slight excess of Al_2O_3. This seems to have been corroborated by the few available data on K_2O vaporization from high CaO slag (see Ref. 4) and by available information on K_2O absorption by high CaO slag under operating MHD conditions (Ref. 5). The systems MgO-$KAlO_2$-SiO_2 and FeO-$KAlO_2$-SiO_2 are ternary over much of their extent, according to existing data (Ref. 6). However, calculation of the high temperature tie line distribution in the more MgO and FeO rich parts of

the systems suggests a marked difference from the $CaO-KAlO_2-SiO_2$ system in that tie lines do not extend from the olivine phases to cubic $KAlO_2$ solid solutions. The effect of increasing X_{FeO} and X_{MgO} on a_{K_2O} may not be as great, therefore. Figure 13 shows data presently available for these systems.

References

1. H. P. R. Frederikse, T. Negas and S. J.Schneider, 1976, Development, Testing and Evaluation of MHD-Materials: NBS Quarterly Report January-March 1976.

2. E. M. Levin, C. R. Robbins and H. F. McMurdie, 1964, Phase Diagrams for Ceramists: Columbus, OH, The American Ceramic Society, p. 156.

3. H. P. R. Frederikse, T. Negas and S. J. Schneider, 1975, Development, Testing and Evaluation of MHD-Materials: NBS Quarterly Report, October - December 1975.

4. L. Cook, E. Plante, T. Negas and R. Roth, 1976, Crystallization and Vaporization Studies on Synthetic Coal Slag Compositions: Proc. 15th Symp. Engineering Aspects of MHD, Philadelphia, PA.

5. J. K. Koester, R. H. Eustis, and M. E. Rodgers, 1976, In-Channel Observations on Coal Slag: Proc. 15th Symp. Engineering Aspects of MHD, Philadelphia, PA.

6. E. M. Levin, C. R. Robbins and H. F. McMurdie, 1964, Phase Diagrams for Ceramists: Columbus, OH, The American Ceramic Society, p. 270.

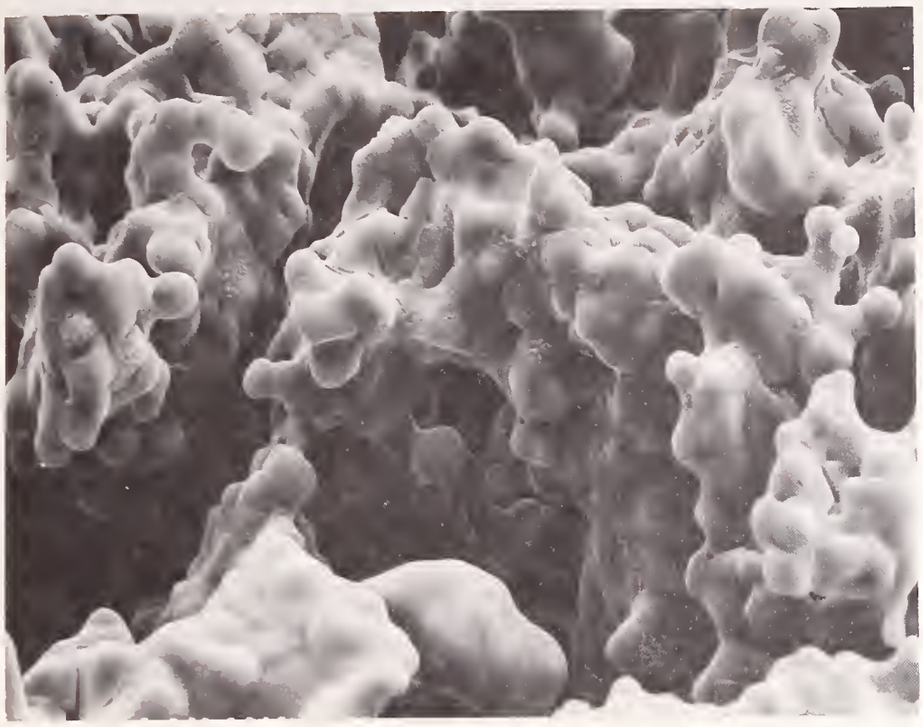

Figure 10a. SEM micrograph (1000X, 20 KV) of $(KAlO_2)_{70}(SiO_2)_{30}$ held at 1880 °C for 10 minutes following pre-equilibration at 1600 °C. Recessed area with deudritic structure is interpreted as devitrified melt.

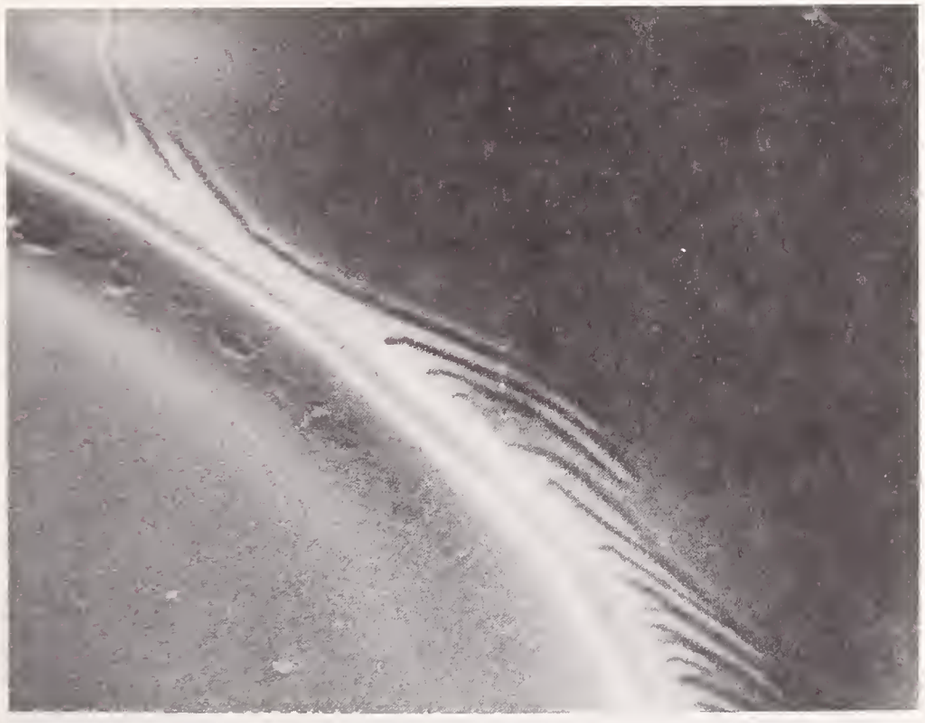

Figure 10b. Enlargement (20,000X, 20KV) of area in upper left of Figure 10a. showing triple grain boundary junction with recessed median suggesting intergranular melt.

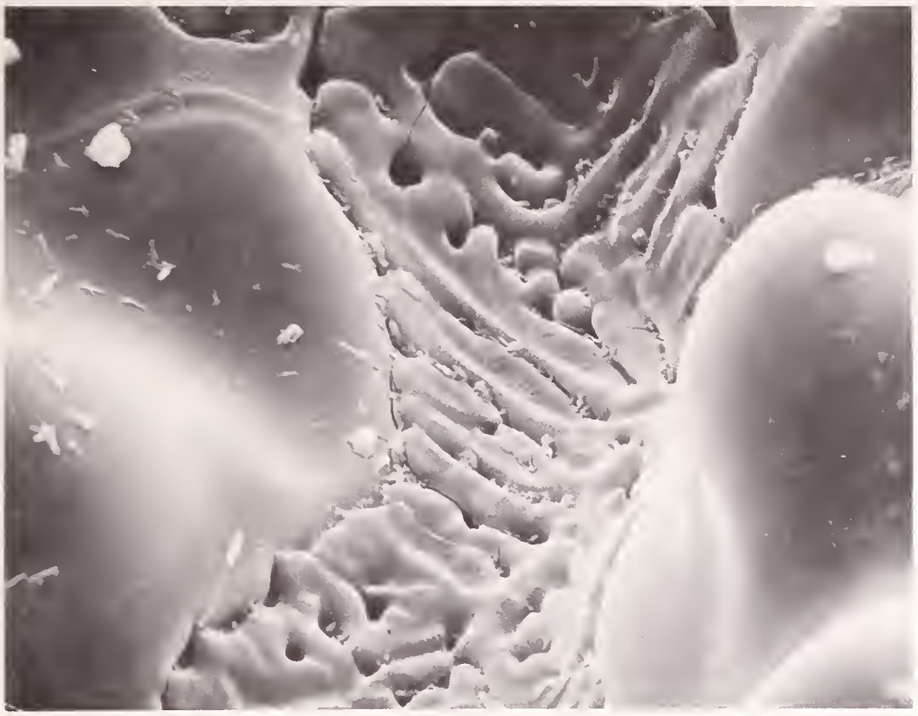

Figure 11a. SEM micrograph (1000X, 20 KV) of $(KAlO_2)_{60}(SiO_2)_{40}$ held at 1850 °C for ∿1 minute following pre-equilibration at 1600 °C. Note rounded grains (mostly tetragonal phase), apparently produced by local melting and recrystallization in response to surface energy minimization requirements.

Figure 11b. Enlargement (20,000X, 20KV) of grain boundary in Fig. 11a. showing no evidence for intergranular melt, in contrast to Fig. 10b.

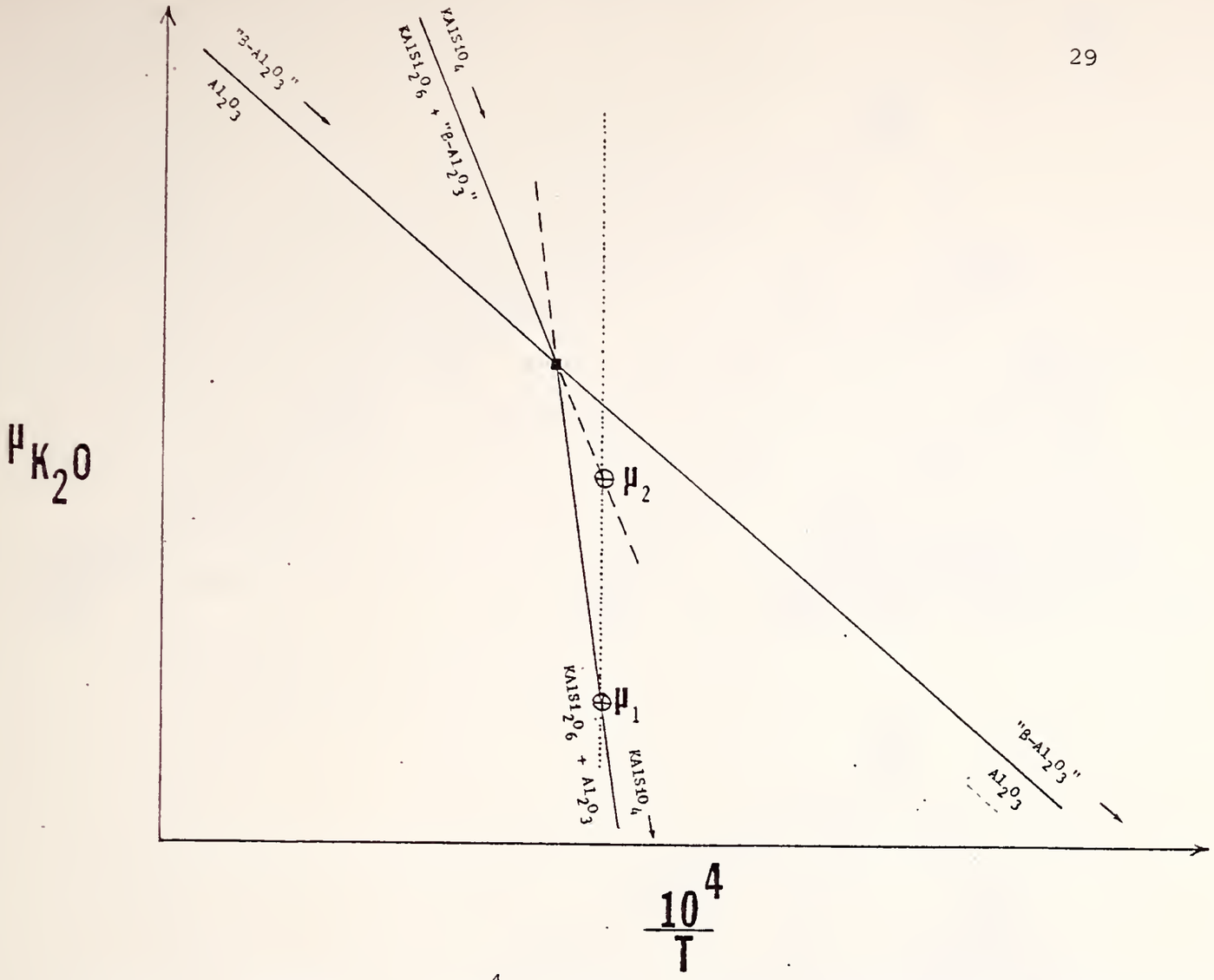

Figure 12. Schematic μ_{K_2O}-$10^4/T$ diagram showing topology of some univariant potassia vaporization reactions of interest. Reactions are univariant only for fixed compositions of phases. Potassia chemical potentials corresponding to the invariant point and above apparently are not attainable under low-pressure experimental conditions.

Intersection of dotted line (Constant T) with reaction lines is indicated by points labelled μ_1 and μ_2. Failing nucleation and growth of α-Al_2O_3, represented by μ_1, vaporization decomposition of $KAlSiO_4$ would be controlled by the metastable extension of reaction involving its decomposition to $KAlSi_2O_6$+ "β-Al_2O_3", represented by μ_2.

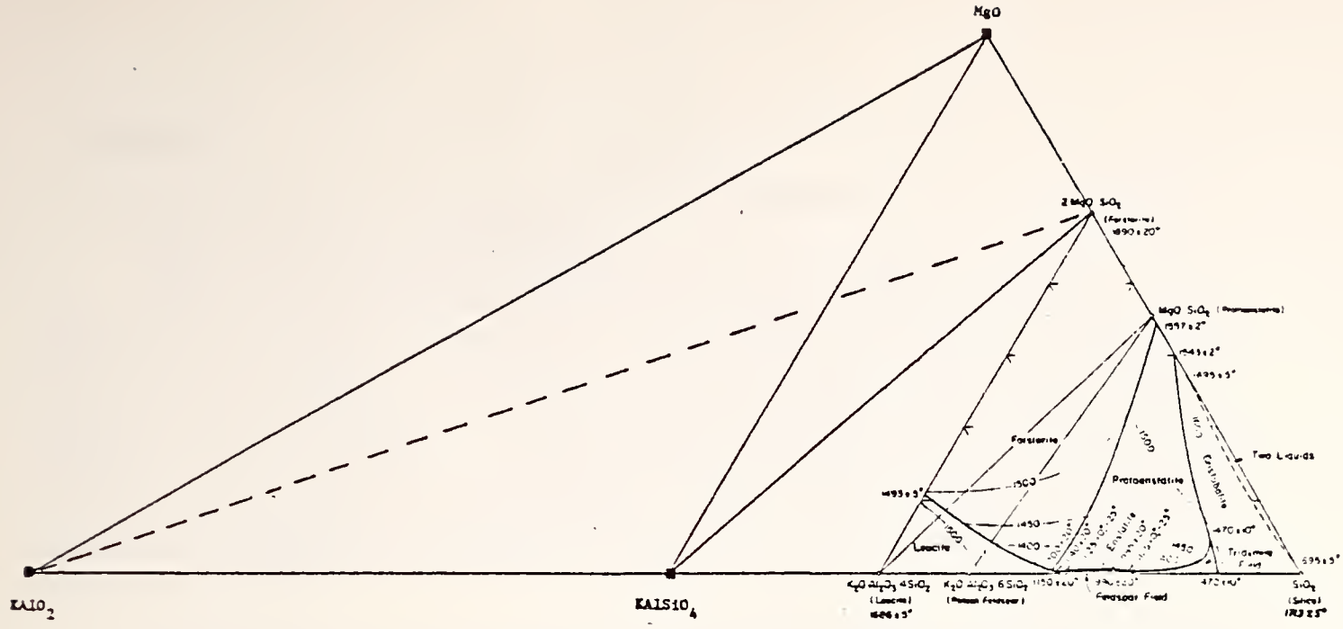

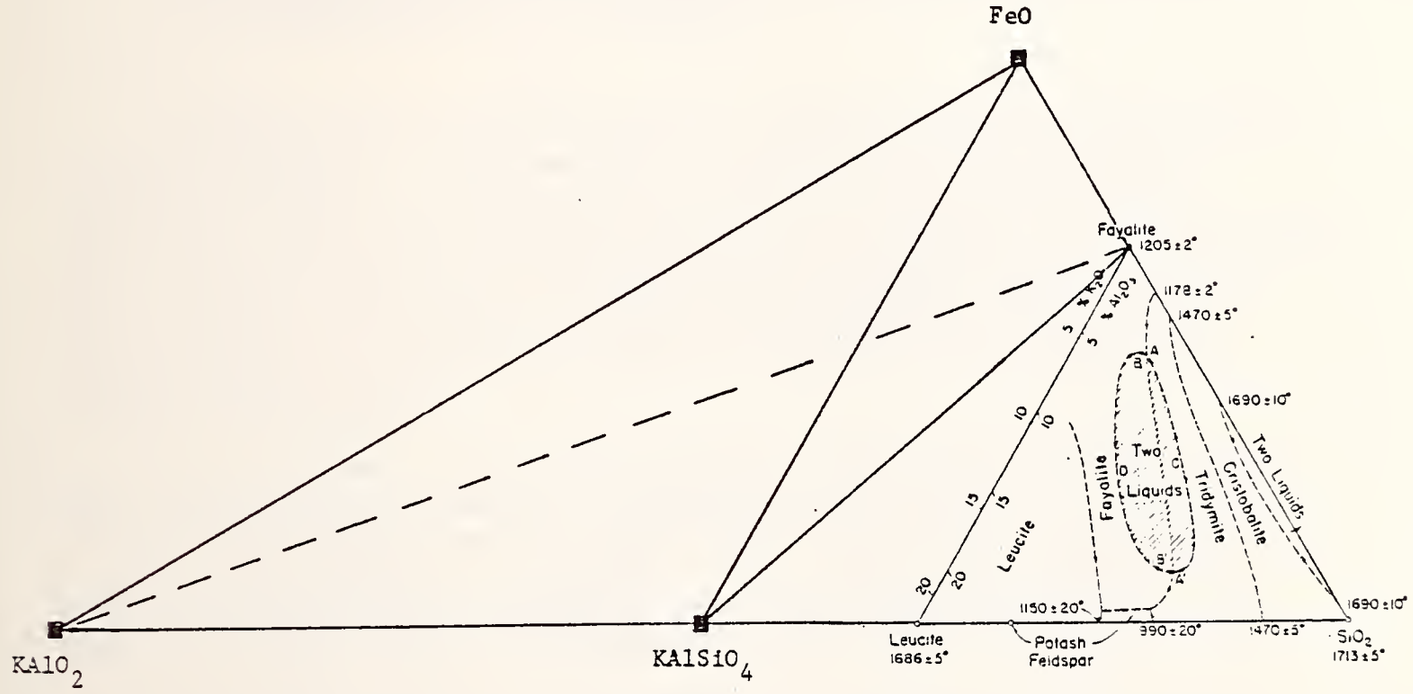

Fig. 13. Phase relations known to date in the systems $MgO-KAlO_2-SiO_2$, $FeO-KAlO_2-SiO_2$ and $CaO-KAlO_2-SiO_2$ (Refs.4,6). MgO,FeO-$KAlSiO_4$ tie lines calculated to be stable at expense of Mg_2SiO_4, Fe_2SiO_4-$KAlO_2$ tie lines.

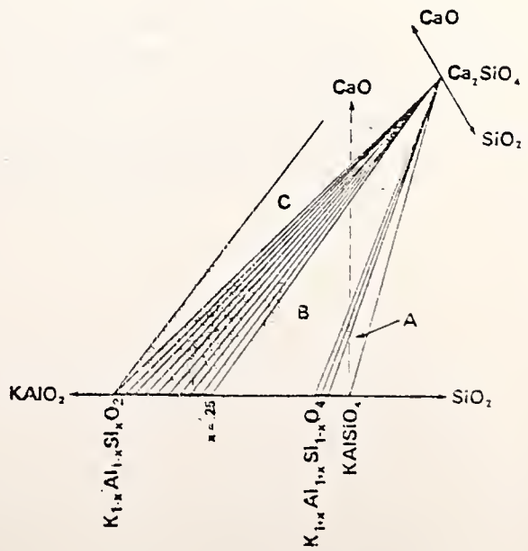

b. Diffusion

a) Diffusion of K into Al_2O_3 (E. N. Farabaugh and J. R. Manning)

Three more diffusion couples were made during this period. All were produced at 1400 °C for 240 hrs. They were ISOA-225 Al_2O_3 (∿83% dense), ISOA-242 Al_2O_3 (∿90% dense) and single crystal Al_2O_3, each was run in its own pellet of β-Al_2O_3. Only the single crystal material has been analyzed to date. Even with the 240 hr. diffusion time, K was detected only to a depth of 2-4μm from the surface of the single crystal. The data was acquired in 2μm steps and after two readings, the level of K X-rays dropped into the background. This time of 240 hours should be sufficient to generate reasonable profiles in the other two Al_2O_3 ceramic specimens.

b) Examination of Diffusion in Magnesia-Aluminum-Iron Spinel Electrode and Magnesia-Aluminum Spinel Insulator Material (E. N. Farabaugh, J. R. Manning and A. J. Armstrong)

Because of the current interest in $MgAl_2O_4$-Fe_3O_4 solid solutions as electrode materials, measurements of interdiffusion between $MgAl_2O_4$ insulator material and $MgAl_2O_4$-Fe_3O_4 electrode material were made. Sandwiches of electrode-insulator-electrode were prepared, heated and examined to track the diffusion of Fe from the electrode into the insulator. Since the iron concentration controls the electrical conductivity in these materials, diffusion of iron from electrode to insulator could strongly affect the operation of both the electrode and insulator in operating MHD channels.

Fig. 14a shows, at 50 X, the insulator (left side) electrode (right side) interface. This sample was produced after diffusion at 1600 °C for 4 hours in the absence of an electric field. Note that the iron spinel is more porous than the pure spinel. Thus, there was no problem in defining roughly where the boundary was. Fig. 14b is an Fe map of the same area showing slight penetration of Fe into the insulator.

A detailed Fe concentration profile was obtained by collecting data at intervals of 150μm, in the region far from the interface, to 20μm in the regions of the interface to trace the diffusion of Fe into the insulator. Fig. 15 shows the plotted data. The concentration of Fe is constant in the electrode until the interface is approached. Then, the concentration drops then rises again just before we enter the $MgAl_2O_4$ insulator. The electrode-insulator interface is indicated by the arrows. The Fe has penetrated ∿0.3mm into the insulator while the electrode shows a depletion band of ∿0.4mm as measured from the curve.

Fig. 16 shows the data collected from a 51 hr test at 1600°C with no electric field. In this specimen we were able to traverse both electrodes and the insulator. Again, we see the build up of iron in the electrode just outside of this electrode-insulator interface. Here the penetration of Fe is ∿0.7mm from each of the insulator-electrode interfaces. The depletion band in the electrode is also ∿0.7mm.

Because of the observed difference in porosity, the transition from electrode to insulator can be seen on the SEM viewing screen while the data is being collected, so the position of the apparent boundary can be easily and accurately established. We say apparent because there is the possibility that some grain growth or sintering has occurred between the two spinel pieces. This would make the apparent boundary move into the insulator if the electrode material grew at expense of the insulator material. It would be possible that the peak in the Fe profile appears where the boundary originally was and was produced by Fe moving to this boundary in a manner comparable to impurities moving to the boundaries of grain in grain growth processes. Alternately, there may be a significant surface barrier preventing or retarding interdiffusion at the boundary. One way to help examine this apparent boundary-related effect would be to do experiments with the original boundary marked with fine wires. The fact remains, however, that there has been an Fe pile up in the boundary region. This effect can only enhance the lifetime of the insulator material in an actual test run.

Further investigations of these spinels are planned including testing the insulator-electrode 'sandwich' at different temperatures and with an applied electrical field.

Calculations of diffusion kinetics in MHD electrode materials have been oriented to concentrate on diffusion in these spinel materials. Diffusion of probability estimates for interdiffusion of Fe and Al on the octohedral spinel sites are being made.

Fig. 14a. 50X secondary electron micrograph showing the $MgAl_2O_4$ insulator on left and iron $MgAl_2O_4$ on the right.

Fig. 14b. Iron area map of the same region.

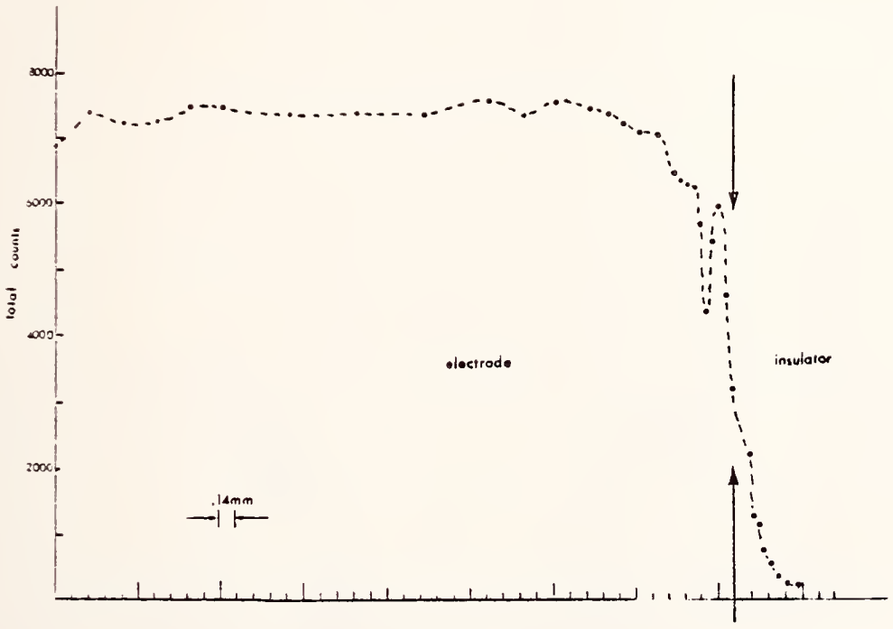

Figure 15. Iron profile taken for 4 hr. test.

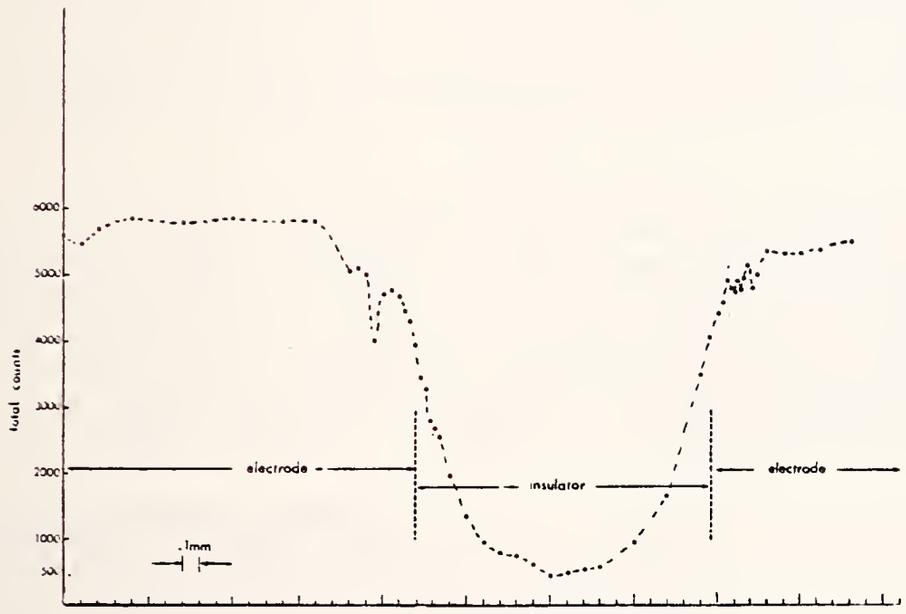

Figure 16. Iron profile taken from 51 hr. test.

Task K. MATERIALS TESTING AND CHARACTERIZATION

a. Spinel Electrodes for a 100-hour Proof Test (W. R. Hosler, H.P.R. Frederikse)

In the early months of 1976, NBS was asked to supply a number of Mg-Al-Fe-spinel samples for testing in the Reynolds MHD test rig under auspices of Argonne National Laboratory. This material is one of the spinels (described in an NBS paper presented at the 15th Annual Symposium on Engineering Aspects of MHD, May 1976, Philadelphia) that holds promise as an electrode material, because of its reported corrosion resistance to slag and seed, reasonably high melting point, and good electrical conductivity between 500 and 1900 °C. Originally, the required electrode assembly, [including preparation of the electrode ceramic, mounting in a suitable electrode holder (with watercooling and electrical lead-outs) and assembling with the appropriate interelectrode insulators] would be designed and built by one or another of the several ERDA-contractors involved in MHD development. However by early May it became obvious that NBS itself had to assume responsibility for the construction of the electrode-insulator test assemblies.

It should be realized, however, that NBS does not have the industrial fabrication facilities required for building such a device. Although this electrode/insulator system is relatively small, one needs all the necessary tools for the preparation of appropriate oxide powders, sintering and hot-pressing of ceramic bodies, flame- and/or arc-spraying equipment to produce ceramic or metallic layers, as well as know-how and apparatus for joining ceramic samples to a metallic base.

In order to have these electrodes built in the limited time prescribed by the test schedule, NBS contacted two companies. The first one, Trans-Tech, of Gaithersburg, MD, supplied the powders and ceramic bodies to our specifications, while both this company and a second one, Technetics of Milford, CT, developed methods for making a very strong ceramic/metal bond. With the assistance of these two companies a dozen electrode/insulator assemblies were built and delivered to the MHD-test facility for testing in September 1976 under Argonne auspices. Details of the construction are given below.

Electrode/Insulator Assembly

Requirements: The test conditions and dimensional limitations as specified by Argonne National Laboratory are as follows:

- two electrodes plus three insulators (cathode),
- two electrodes plus three insulators (anode),
- assembled with appropriate copper sample holders (water-cooled).
- length of electrodes: ∿3 in.
- width of electrodes: 0.375 in.
- height of electrodes: 0.1-0.5 in.
- insulator width: 0.05 - 0.10 in.

Two sets of the above.

- Surface temperature of electrode between 1800 and 2200 K;
- Average heat flux: ∿100 W/cm^2.

The test is supposed to last for 100 hrs. with "normal" start-up and shut-down times of 30 min. each.

Design: The electrode material chosen for this test is the Mg-Al-Fe-spinel ($3MgAl_2O_4$-$1Fe_3O_4$, now known as "MAFF-31").

The electrical conductivity as a function of temperature is given in the 4th Quarterly Report (Fig. 1, p. 12).

The thermal conductivity was measured by Dr. J. Lambert Bates (Battelle NW); data are presented in Table A.

The thermal expansion of this spinel is about 8-9 x 10^{-6} at 1000 °C.

The most important design parameter is the interface temperature between the spinel ceramic and the metal or metal alloy base. Because of sufficient electrical conductivity of the spinel down to rather low temperature, this temperature was chosen to be about 600-700 °C. Using the required surface temperature and heat flux, and the measured thermal conductivity of the spinel, the thickness should be of the order of 3.0 - 4.0 mm.

As a result of this small spinel thickness another problem arises: How to attach the ceramic firmly to the metal base? Considering the 1000-1100 °C temperature difference across 3.5 mm of the spinel ceramic, it is clear that the thermal expansion at the top surface will be much higher than at the bottom. Hence, the strains in the ceramic layer will be very large, resulting in a tendency for "bowing" and spalling.

To solve this problem two different approaches have been used.
a. The metal-felt pad (Technetics)
b. The cermet layer(s) (Trans-Tech)

Construction:
a. Details of the electrode/insulator assembly using the metal-felt pad are shown in Figure 17. The metal-felt is a wire-mesh material made of an Fe-Cr-Al alloy. It is difficult to determine the thermal conductivity of this material; the best estimate is 0.015 - 0.025 W/cm.deg. (between) 100 and 600 °C). Hence, a thickness of 1.5 mm is required to reach a felt-spinel interface temperature of 600 °C. In order to avoid cracking and spalling of the spinel ceramic as much as possible, it was decided to limit the length of the ceramic and hence to build the three-inch electrode out of 3 one-inch "tiles".

The fabrication followed a series of steps. First, 1.5 mm thick metal-felt pads were brazed to the individual 4 mm thick copper tiles. Subsequently, a 3.5 or 4.0 mm thick layer of spinel was gradually built-up on the metal-mesh using the flame spraying technique. After shaping and trimming of these composites, a set of three "tiles" was brazed to the water-cooled copper electrode holder. Final assembly of the electrode system will be achieved by placing three insulator plates (pure dense $MgAl_2O_4$) on each side of the electrodes and attaching them with RTV-cement.

b. The construction of the electrodes using the cermet joining technique is quite similar. Instead of the metal-felt, the metal and the ceramic are connected by building up several layers of different metal-ceramic mixtures (cermets). For instance, one can flame-spray first a layer of

TABLE A. Thermal Conductivity of $3MgAl_2O_4 \cdot 1Fe_3O_4$

Temperature (°C)	Temperature (K)	λ (W/cm·deg)
527	800	.0317
577	850	.0319
627	900	0.0313
727	1000	.0301
827	1100	.0290
927	1200	.0279
1027	1300	.0270
1127	1400	.0262
1227	1500	.0255
1327	1600	.0246
1427	1700	.0237
1527	1800	.02233

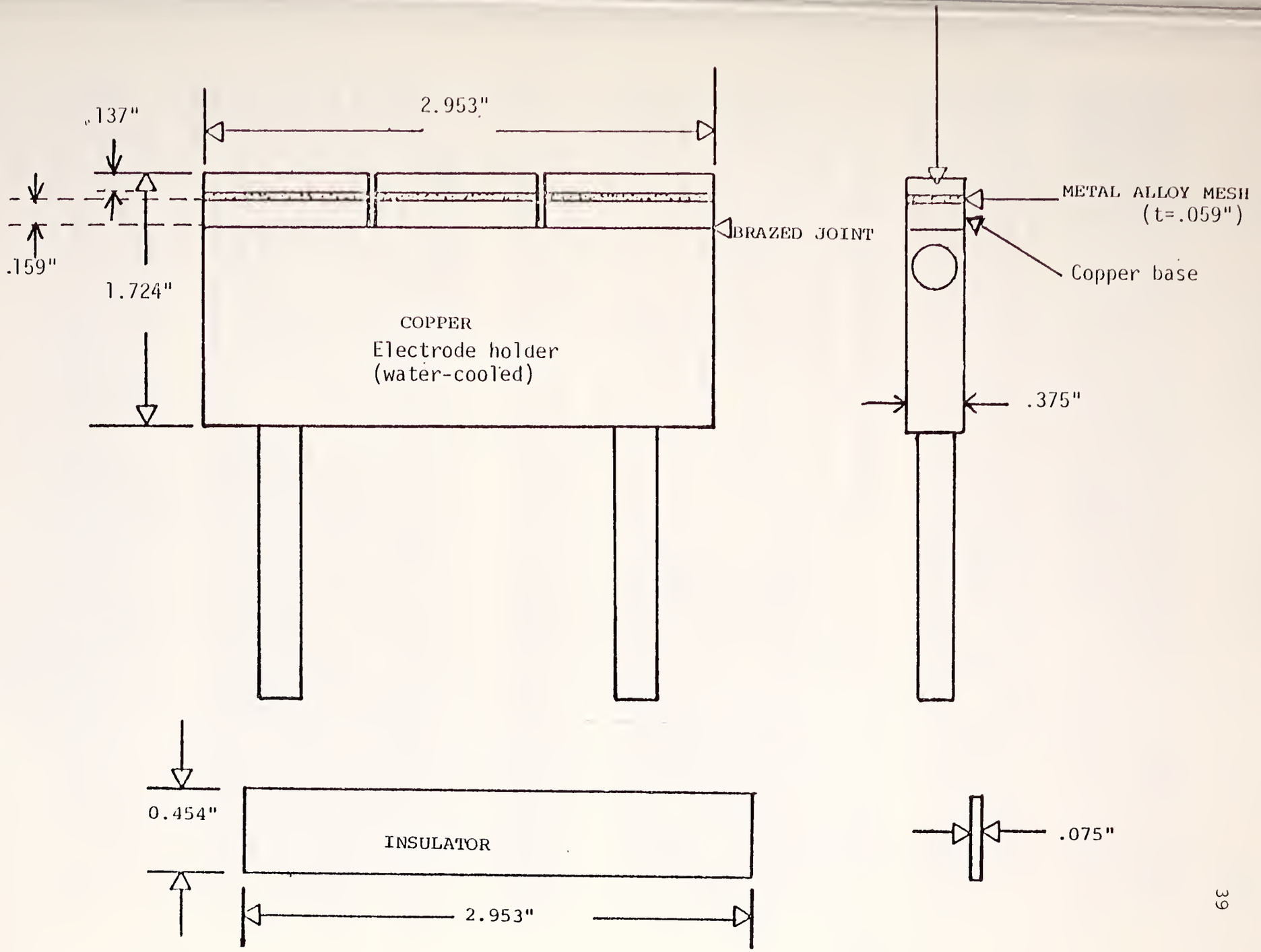

Fig. 17. Design of spinel electrodes for ANL-Reynolds test.

metal powder, and then one containing about 25% of the ceramic powder. This is followed by a 50-50 and then a 75-25 mixture. Finally, a layer of 100% Mg-Al-Fe spinel is deposited. The total thickness of these graded layers is small (much less than 1 mm). On top of the cermet the ceramic is built-up until the desired thickness is reached.

It should be understood that the particular fabrication methods and dimensions chosen for this set of electrode/insulator assemblies are not necessarily optimized in all respects. Many variations within the general framework of this approach are possible. NBS is cooperating with appropriate groups to optimize these electrodes for use in ERDA channel development programs.

b. U-02 MHD Materials Test (Phase II) (W. R. Hosler, A.J. Armstrong, T. Negas)

During this reporting period some time was spent on several aspects of the preparation for the joint US/USSR MHD-Materials Test (Phase II) to be conducted in the U-02 facility in Moscow. The module (electrode and cathode), constructed by Westinghouse is similar to the one built for the Phase I test (Sept. 1975). However, the electrode materials, the lead-outs, the method of attachment, and the segmentation are different. The overall length is ∿490 mm divided in 6 groups of 5 electrodes. Each group (with one exception) contains 5 materials of identical chemical composition: the last 3 groups include electrodes fabricated by two or more suppliers (see Figure 18).

Mr. Hosler, who will participate in the U-02 test (Phase II) as one of the 6 U.S. monitors, collaborated with Westinghouse staff members in the preparation of the Work Plan and in arranging appropriate shipping procedures.

Powder Preparation. In cooperation with Trans-Tech Inc. sinterable powders of conducting $3MgAl_2O_4{:}Fe_3O_4$ spinel solid solution were developed and have been utilized by Battelle Northwest and Trans-Tech Inc. to prepare electrodes for testing in U-02, Phase II. Grain size and phase composition were monitored and characterized by SEM and x-ray diffraction analysis throughout all stages of development. We are now investigating the preparation of powders for several other Mg/Al/Fe-oxide spinel solid solutions. Dense, sintered, ceramics are being prepared for electrical conductivity measurements. We envision utilizing compositions lower in iron content (hence, higher melting point) in a "graded" Mg/Al/Fe-oxide spinel electrode provided that adequate electrical conductivity can be demonstrated.

Pre-test Characterization. A number of measurements, required for pre-test characterization, were made on all samples for the U-02 test. The results of these experiments [electrical conductivity (p. 11), structural and chemical information (Table B)] were assembled and have been transmitted to the USSR-side before the start of the test.

Fig. 18 UO2 MODULE ELECTRODE IDENTITY

Supplier	Lead-out		ASSIGNED CURRENT DENSITY (A/cm^2)		Supplier	Lead-out	
W	Pt	1101	1.5	2101	W	Pt	GRADED
"	"	1102	.8	2102	"	"	CeO_2 — ZrO_2 — Ta_2O_5
"	"	1103	.8	2103	"	"	35 65
"	"	1104	.8	2104	"	"	50 50
"	"	1105	0	2105	"	"	75 25
							78 20 2
W	Inconel	1206	0	2206	W	Inconel	GRADED
"	"	1207	.8	2207	"	"	CeO_2 — ZrO_2 — Ta_2O_5
"	"	1208	.8	2208	"	"	35 65
"	"	1209	.8	2209	"	"	50 50
"	"	1210	1.5	2210	"	"	75 25
							78 20 2
W	Pt	1311	1.5	2311	W	Pt	
"	"	1312	.8	2312	"	"	
"	"	1313	.8	2313	"	"	$50CeO_2$ — $50ZrO_2$
"	"	1314	.8	2314	"	"	
"	"	1315	0	2315	"	"	
BNW	Cu	1416	0	2416	BNW	Cu	
"	"	1417	.8	2417	"	"	$75MgAl_2O_4$ — $25Fe_3O_4$
"	Pt	1418	.8	2418	"	Pt	
Trans-Tech	Pt	1419	.8	2419	"	"	
BNW	Cu	1420	1.5	2420	"	Cu	
BNW	Pt	1521	1.5	2521	BNW	Pt	$75MgAl_2O_4$ — $25Fe_3O_4$
"	"	1522	.8	2522	"	"	
LASL	Cu	1523	.8	2523	LASL	Cu	$FeAl_2O_4$ — Fe_3O_4
MIT	Cu	1524	.8	2524	MIT	Cu	
MIT/LASL	Cu	1525	1.5	2525	MIT	Cu	
G.R.	Cu	1626	1.5	2626	G.R.	Cu	
"	"	1627	.8	2627	"	"	$LaCrO_3$
W	"	1628	.8	2628	W	"	
G.R.	Pt	1629	.8	2629	G.R.	Pt	
W	Cu	1630	0	2630	W	Cu	

CATHODE

PLASMA FLOW

ANODE

W - Westinghouse
BNW - Battelle Northwest
LASL - Los Alamos Scientific Lab.
G.R. - General Refractories

TABLE B

Summary of Pre-test, U-02, Phase II Materials

Material	X-ray Diffraction Analysis (phases)	SEM/EDX analysis (impurity)
Spinel $3MgAl_2O_4:Fe_3O_4$ solid-solution (Trans-Tech Inc.)	Single-phase, well-crystallized spinel $\underline{a}$=8.185Å. Powders of this material prepared in air yield $\underline{a}$=8.160Å. This together with the fact that this material (unlike the "in air" material is ferromagnetic at room temperature indicates that the Fe^{2+}/Fe^{3+} ratio is somewhat greater than in the "in air" spinel.	None detected as major impurities (0.5-1% level)
Spinel $3MgAl_2O_4:Fe_3O_4$ solid-solution (Battelle NW)	a) Top (plasma side) portion contains well-crystallized spinel, $\underline{a}$=8.185Å (as Trans-Tech material). b) Lower, more porous portion contains at least two spinels, $\underline{a}$=8.185 and $\underline{a}$=8.170.	Cr is the major impurity detected (0.5-1.0%)
Spinel $7FeAl_2O_4:3Fe_3O_4$ solid-solution (Los Alamos)	Poorly crystalline Fe/Al-oxide spinel with $\underline{a}$=8.261Å as the dominant phase. One or more additional spinel phases having larger cell dimensions are also present. Their x-ray lines are too weak and broad for accurate parameter determination.	Domains (<0.07 mm) containing more porous oxide enriched in Al_2O_3 with respect to the denser surrounding spinel matrix. (See Fig. 23).
Spinel $7FeAl_2O_4:3Fe_3O_4$ solid solution (MIT)	Well-crystallized spinel with $\underline{a}$=8.231 Å.	Contains major impurities consisting of K and Si (≤5%). These are distributed throughout the material as porous impurity domains (K+Si) up to ∿0.7 mm. Another set of less dominant impurity centers (up to ∿0.05 mm) consists of Mg and Al concentrations. (see Figs.24, 25).
Graded Cerium oxide-zirconia:Ta (Westinghouse)	The composition range encompassed by this material is described in previous U-02 report.	Dominant impurities (0.5-1.0%) include Al, Si, most of the rare earths, and probably Cs.
$LaCrO_3$:Mg (General Refractories)	Well-crystallized orthorhombic perovskite a = 5.478 Å b = 7.760 Å c = 5.516 Å	Major impurities (0.5-1.0%) include Al and probably Sc as well as most of the rare-earths. Minor impurities (<0.5%) include Si, Ca, and Th.
$LaCrO_3$:Mg (Westinghouse)	same as $LaCrO_3$:Mg above	Major impurities Al, Si, Sc and other rare-earths

The module itself was delivered in Moscow on August 23, 1976; the U-02 test (Phase II) is expected to begin on September 20, 1976 and will last for at least 100 hours. After the test, the module is expected to be brought back to NBS around October 1, 1976; it will be disassembled during the week of October 4 in the presence of several Soviet representatives.

c. U-25 Bypass Channel (H. P. R. Frederikse, S. J. Schneider)

During the Spring meeting of the US/USSR MHD-Steering Committee in June 1976, it was suggested that future tests of electrode materials and generator walls could be conducted in a test channel built as a bypass of the large U-25 generator duct. This bypass channel will be constructed to fit inside a superconducting magnet to be delivered to the USSR in 1977. The magnet will provide a field of 5 Tesla. As far as the channel is concerned, it is intended to be operated with maintenance material added to the fuel, and a mass flow appreciably higher than that of the U-02. The channel would be used both for plasma experiments and wall materials tests. The implementation of these plans will be discussed at the Moscow meeting of the MHD-Materials Group in October 1976.

d. Soviet Test at UTSI (US/USSR MHD-Materials Testing)

Two Soviet electrode materials will be tested in the UTSI MHD facility in early October. This test will be run with coal slag additives. A. J. Armstrong will participate in this test. The two materials are SiC (+ Ti) and Cr-$LaCrO_3$. The first batch of samples has been received at NBS. All but 4 of each (for X-ray measurements) have been forwarded to Dr. Lloyd Crawford at UTSI.

e. AVCO Test (August 1976) (T. Negas, W. Hosler, E. Farabaugh, L. Cook)

In September 1976 we received two anode electrodes from AVCO Corp. for analysis. Stan Petty conducted an MHD test utilizating cooled rectangular copper bars onto which a metal alloy mesh (1.5mm thickness) produced by Technetics Corp. was brazed. The composition of the alloy wire is considered proprietary but contains Fe and Cr as dominant constituents with Al and Si as minor components. One anode mesh was plasma sprayed with a conducting spinel solid solution having the composition $3MgAl_2O_4:Fe_3O_4$. Sprayable powders of this material were prepared by Trans-Tech Inc. The thickness of the sprayed spinel layer was ∿1.0mm. The second anode was sprayed (∿1.0mm) with $80ZrO_2/20Y_2O_3$ from powders of unknown origin. These anodes first were equilibrated in the AVCO test channel with AVCO slag before seed was introduced and power drawn. Test duration in the slag-seed-power mode was 5 hr. Electrode design was by AVCO although the conducting spinel was suggested by NBS.

The two anode bars were "potted" with epoxy and several slices perpendicular to the bar length were sawed from each and lightly polished for analysis by SEM/EDX. Initially, there was some question concerning the direction of plasma flow with respect to anode orientation as received. However, during analysis it became clear that one side of each electrode consistently revealed maximum degradation, particularly of the metal mesh. This side is assumed to be the upstream portion of the anodes where current tends to be concentrated by J x B.

It may be recalled that from the analysis of previous AVCO anodes the nature of the degradation of inconel electrodes could not be deduced definitively as very little anode metal remained after long duration (100 hr.) testing [1]. The results from the present test suggest that localized arcing and heating primarily on the anode upstream side lead to the degradation of anode metal-ceramic components. Both anodes, regardless of the initial, intervening ceramic oxide layer between wire mesh and slag, reveal similar phenomena. The sprayed ceramic layers tend to be discontinuous and crystalline (cold) slag overlies either these layers or is directly on the wire mesh. On the upstream side where slag mainly overlies metal mesh the alloy is degraded (oxidized) but not extensively for this short test. On the downstream side the alloy remains relatively unaltered whether covered by ceramic plus slag or mainly crystalline slag without ceramic. These observations suggest that slag dissolves the ceramic oxides (particularly the ZrO_2-based material) with or without high current activity. However, degradation of the wire mesh is apparent only in the upstream high current density region.

Figure 19a is typical area (150X) revealing the wire mesh-ceramic oxide ($80ZrO_2/20Y_2O_3$)-slag interfaces. Figure 19b, a corresponding map for Zr, clearly shows what remains of the sprayed zirconia layer. Wire under the remaining zirconia (at right) remains in relatively good condition. Where zirconia is nearly absent (at left) the area has been invaded by slag components (K and Si) and the wire was subjected to oxidation. This is illustrated by Figs. 19c (K map), 19d (Cr map) and 19e (Fe map). Notice (Figs. 19d and 19e) that for this alloy composition the Cr component is particularly sensitive to oxidation.

Figure 20a (100X) is a typical area showing the wire mesh-ceramic oxide ($3MgAl_2O_4$:Fe_3O_4 spinel)-slag interfaces. Here the remaining spinel has a maximum thickness of 0.2-0.3mm and the underlying wire is in relatively good condition. Figure 20b (Mg map) and Figure 20c (Si map) reveal the spinel-slag interface. Figure 21 (190X) is an adjacent upstream area of the anode. Here an interface between two unlike materials exists along the vesicular zone running north-south about midway in the figure. Figure 22a is a magnification (500X) of a portion of this interface. Included is a wire remnant also shown in Figure 21. Figure 22b (Si map) reveals the position of the lower portion of the slag layer. Figures 22c (Fe map) and 22d (Cr map) show that under the slag is a zone of oxidation enriched with Fe and particularly Cr, the dominant wire components. The spinel phase is practically absent. Notice, as before, that the wire remnant is depleted in Cr.

Several conclusions can be drawn from these data as well as other extensive photographic evidence available but not presented. These include:

1. a rather sharp interface can and does exist between AVCO slag (crystalline or glassy) and sprayed ceramic suggesting compatibility after considerable recession of the latter;

2. this ceramic-slag zone, however, is discontinuous and practically absent at the anode upstream side where the wire mesh is subjected to oxidation, particularly for the zirconia-mesh anode; and

3. this correlation indicates that localized, excessive heating and high current density associated with arcing result in,

   a) solution/incorporation of the sprayed ceramic into/by the slag phase, and

   b) oxidation of the underlying wire mesh, probably without melting of this particular alloy.

It may be supposed that conducting ceramic oxides thicker than ∿1mm may be more beneficial to "protect" underlying metal anodes. However, if arcing proceeds through slag-ceramic-metal interfaces, even greater thicknesses should be subjected to similar destruction. In the arcing mode, therefore, the situation boils down ultimately to slag on metal whereupon the properties of the metal become overwhelmingly important.

It should be noted, however, that a comparison of the sprayed zirconia and spinel anodes reveals that, for this short test, the latter (better conducting) material appears to be beneficial in terms of "spreading out" current distribution. The zirconia anode shows evidence for current concentration only on the upstream side.

We also received from AVCO unoriented samples of "slag" from tested (20 hr) cathodes consisting initially of metal(?)-hercynite (Fe-Al oxide spinel solid solution of unknown bulk composition). The material proved to be nearly identical with slag from cathodes analyzed in reference [1]. Hercynite-type spinel was not found. Two tested cathodes consisting of the above materials also were received at the end of this reporting period. Analysis is in progress.

REFERENCE

[1] Analysis of AVCO Mark VI C Channel Electrodes After Long Duration Test, W. R. Hosler, T. Negas and S. W. Petty, Proceedings 15th Symposium on Engineering Aspects of Magnetohydrodynamics, Philadelphia, PA, May 24-26, 1976.

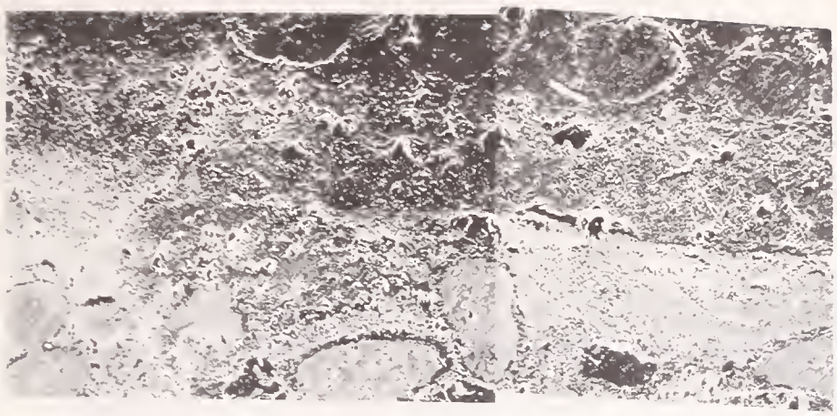

Fig. 19a. Anode (150X, upstream area) consisting of metal alloy (Fe, Cr) mesh (bottom), the remains of a $80ZrO_2/20Y_2O_3$ sprayed layer and slag (top).

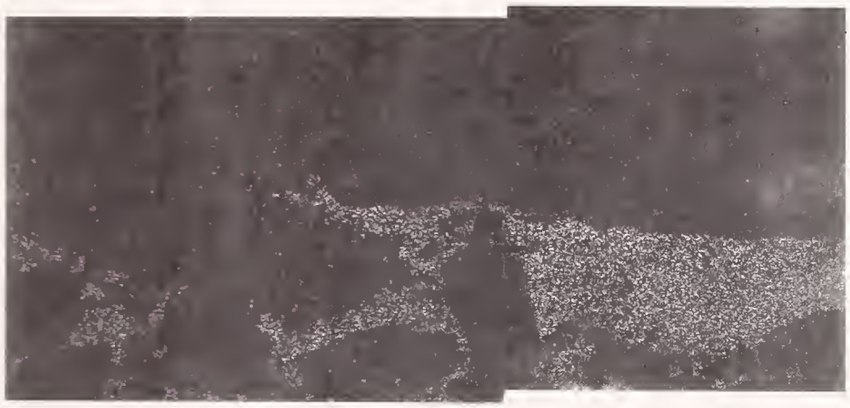

Fig. 19b. Elemental map for Zr of area in Figure 19a.

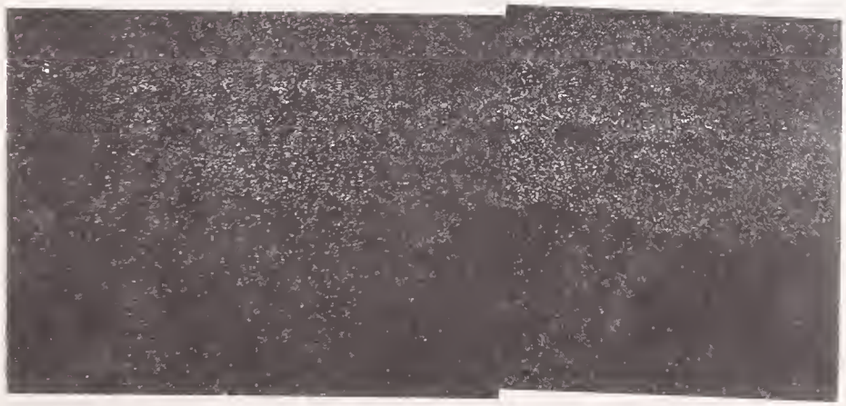

Fig. 19c. Elemental map for K of area in Figure 19a.

Fig. 19d. Elemental map for Cr or area in Figure 19a.

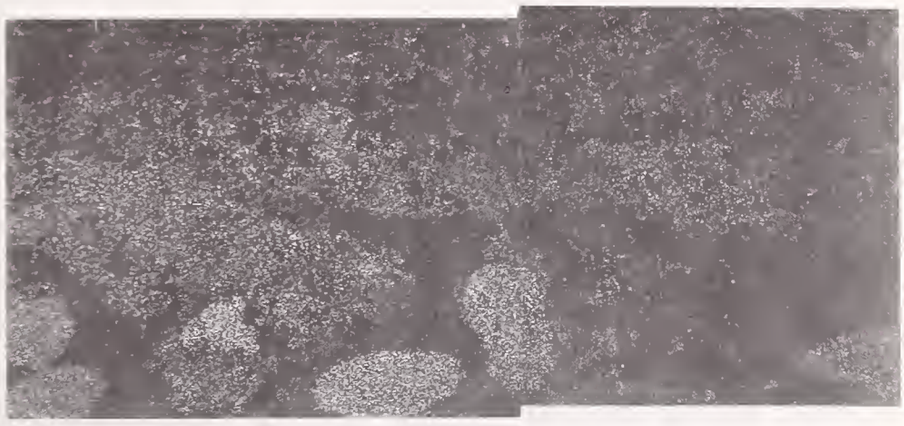

Fig. 19e. Elemental map for Fe of area in Figure 19a.

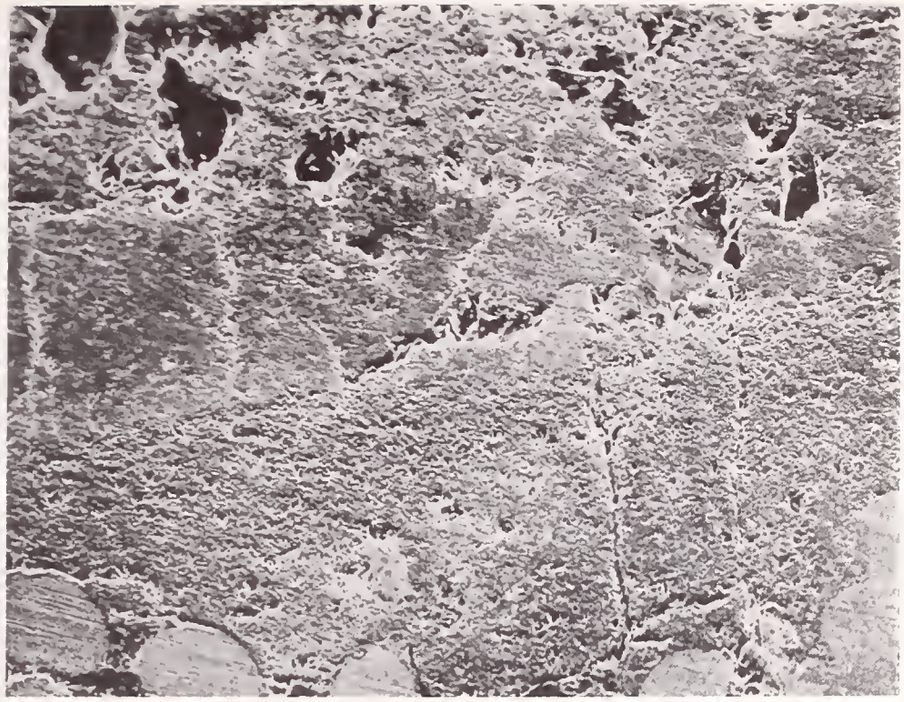

Fig. 20a. Anode (100X) consisting of metal alloy mesh (bottom), the remains of a conducting spinel layer (see text) and slag (top).

Fig. 20b. Elemental map for Mg of area in Fig. 20a showing position of slag layer.

Fig. 20c. Elemental map for Si of area in Fig. 20a showing the slag layer.

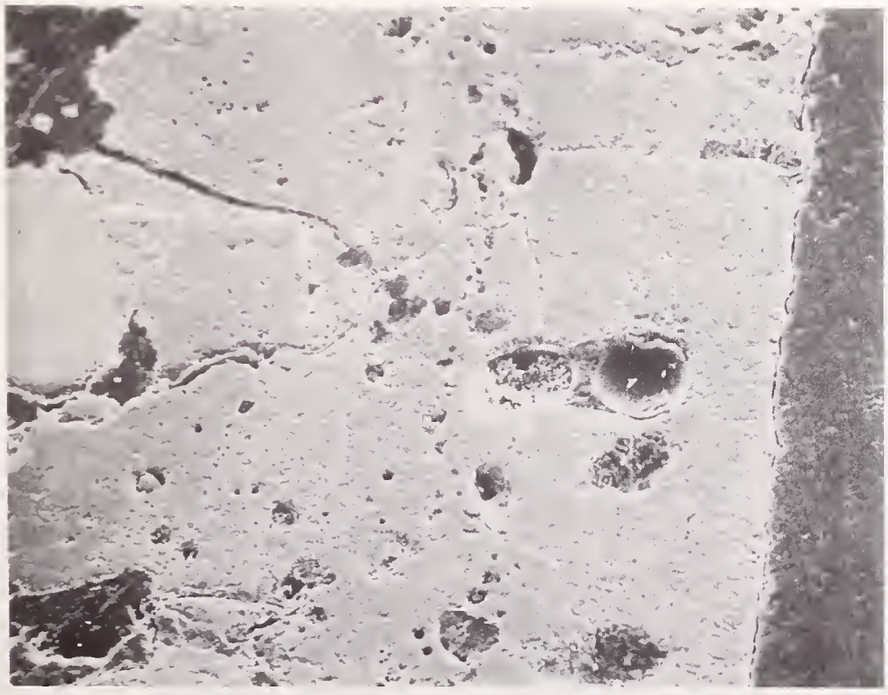

Fig. 21. Anode (190X, upstream area) adjacent to area in Fig. 20a showing wire, oxidized wire and slag.

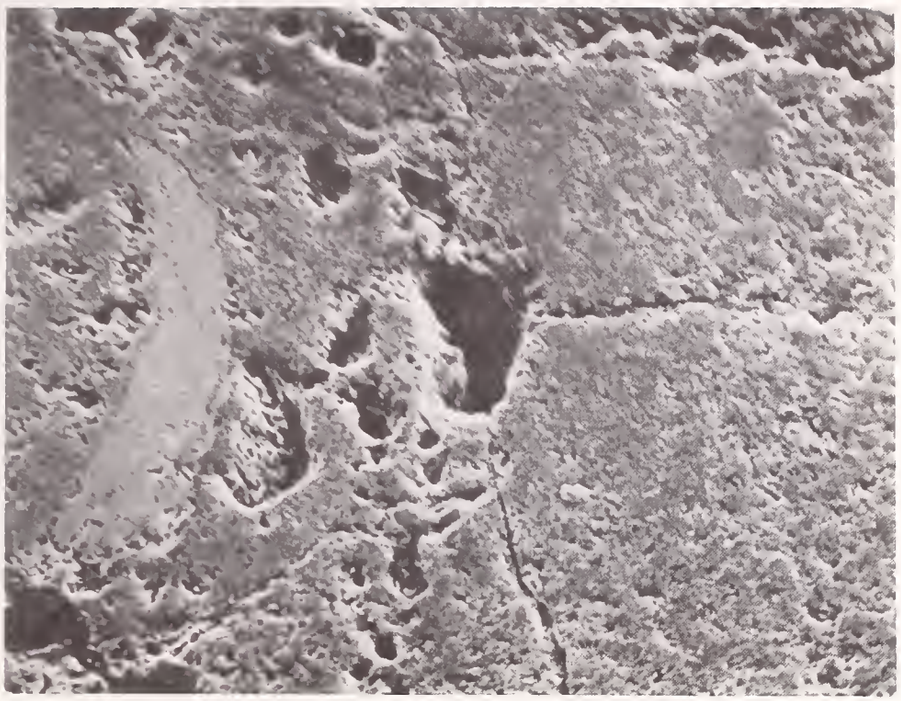

Fig. 22a. Manification (500X) of portion of area in Fig. 21.

Fig. 22b. Elemental map for Si of area in Fig. 22a.

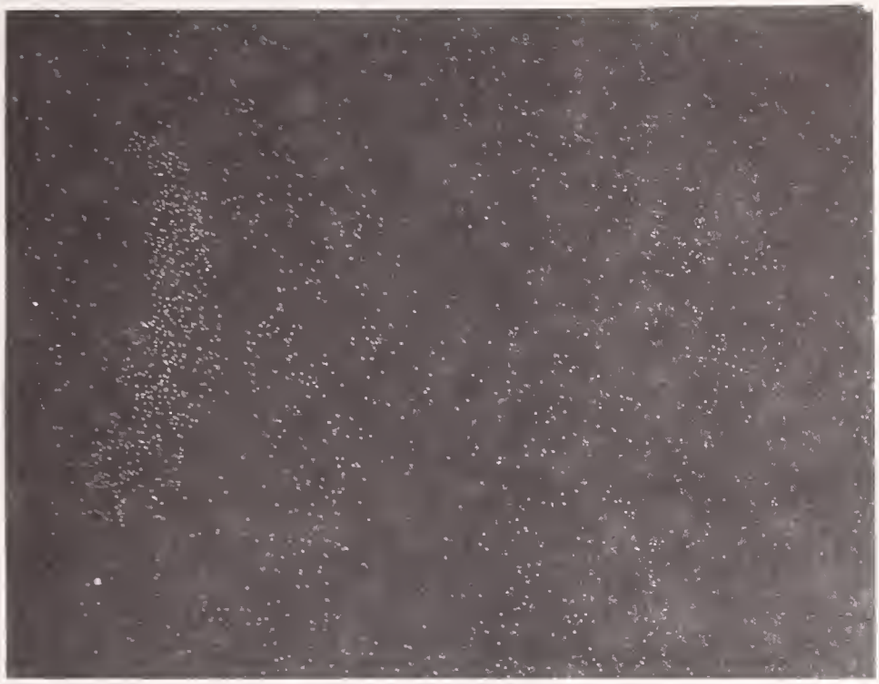

Fig. 22c. Elemental map for Fe or area in Fig. 22a.

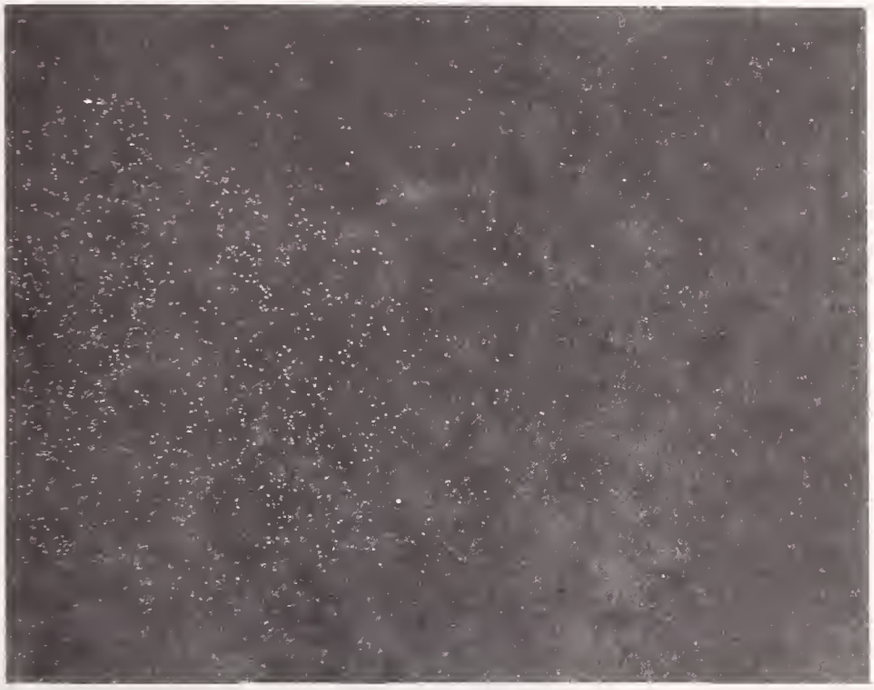

Fig. 22d. Elemental map for Cr of area in Fig. 22a.

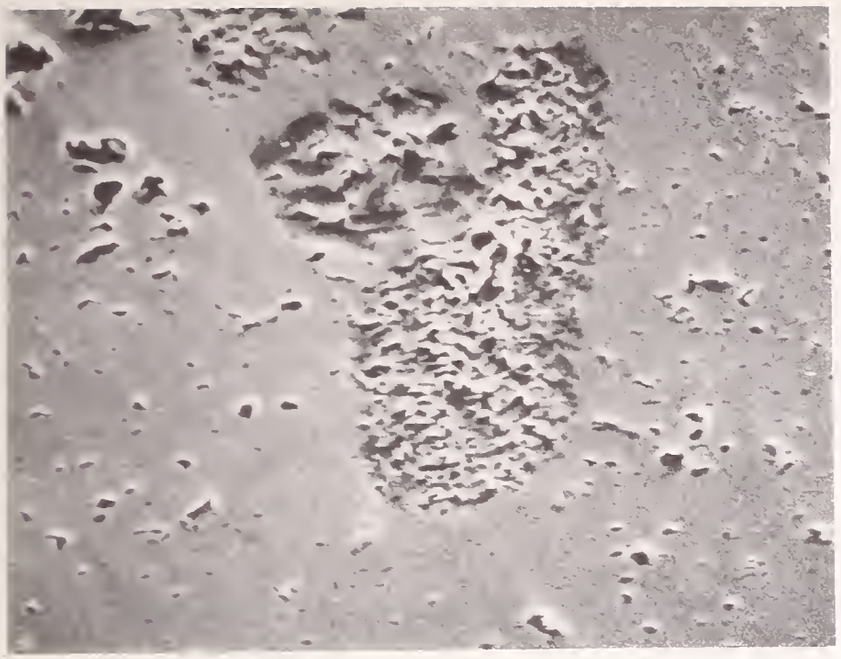

Fig. 23. Typical Al-rich domain (1000X) in Fe/Al-spinel prepared at Los Alamos.

Fig. 24. Typical Mg/Al-rich domain (2000X) in Fe/Al-spinel prepared by MIT.

Fig. 25. Typical K/Si-rich domain (1000X) in Fe/Al-spinel prepared by MIT.

f. SEM Examination of Corhart X-317 Ceramics (Magnesia Spinels) Tested at FluiDyne Eng. Corp. (E. N. Farabaugh and D. B. Minor)

One of the most promising preheater materials is the Corhart X-317 spinel. Specimens of the materials tested under different experiment conditions have been examined. The object of these studies during this reporting period has been to determine the depth of penetration of different elements into the spinel, to identify elements in the reacted area, and to determine which of the two phase MgO and $MgAl_2O_4$, present in the X-317 materials, is being predominately reacted in the near surface volumes.

Specimen FN-27 (Cohart X-317) was run at 1800°K for 30 hours in the presence of ash and seed. SEM mapping and EDX work has shown that the reacted layer is ∿0.4mm thick. Its microstructure has more large pores than in the bulk of the specimen. Thus, one can roughly determine the limits of the reacted layer by noting the position where the change in microstructure is seen. This is shown in Fig. 26 where the arrows indicate the extent of the reacted layer.

Elemental concentrations of Mg, Al, Si, Ca, K, Cr, and Fe were found in the reacted layer. The concentration of Mg increased as one moved from the surface through the reacted layer into the bulk of the material where it leveled off. Al concentrations varied but essentially stayed within fixed limits over the same region. The x-ray peaks for Si, Ca, K, Cr, and Fe all decreased as the layer was traversed, falling to near background at distances of twice the layer thickness (∿.8mm).

To address the problem of which phase is reacting predominately, x-ray mapping was done on a portion of the reacted layer shown in Fig. 27a. Fig. 27b is an Al map, 27c is a Ca map, 27d is a Si map and 27e, a map of the same area. Note that in 27b we see areas with no Al concentrations. These areas are filled in with Ca and Si as shown in 27c and 27d. In 27e there is no large concentration of Mg associated with these areas. A possible explanation of these features is that the Al-free areas in 27b were originally MgO grains. The area diameter, ∿40 μm, is about the right size for MgO grains found in the untested material. Upon testing, Si, Ca, K, and Mg may react so as to attack these MgO grains forming other phases in their place. This would explain the lower concentration of Mg in the reacted layer relative to the bulk, as well as the appearance of the elemental maps.

To check this idea further, part of the specimen in the bulk (4-5 mm from the surface) was examined. The region is shown in Fig.28a , where we can see the outline of grains in the surface. Fig. 28b is an Al map of the same area showing that the grains outlined in 28a coincide with the Al-free regions in 28b. Fig. 28c is an Mg map of the same region. The high Mg concentration coincides with the grains of 28a. Thus we can

conclude the grains are MgO. This type structure was reacted in the gas streams to produce that shown in Fig.27a during its test. These results suggest that the MgO is preferentially reacted compared to $MgAl_2O_4$ in the test. $MgAl_2O_4$ also is reacted, but not to the extent that the MgO grains are.

X-ray data taken by A. Perloff tend to support this explanation. Powder made from the reacted layer showed less MgO relative to $MgAl_2O_4$ than powder made from the bulk of the specimen.

A micrograph taken from specimen FN-65 (Corhart X-317) tested for 30 hrs. with ash and seed and cycled between 1800°-1600°K is shown in Fig. 29a The depth of penetration was ∿.3mm. Maps of the same region are shown in 29b for Mg, 29c for Al, 29d for Si. Again the Mg deficient reacted layer is seen, suggesting the preferential reaction of MgO with gas stream components. Fig.29c shows a more uniform distribution of Al in the reacted layer than in the bulk, suggesting the $MgAl_2O_4$ has also reacted. 29d shows the higher concentration of Si in the layer. Elemental constituent of the layer were Si, K, Ca, Mg, Al, Cr, and Fe.

Fig.30 is a micrograph of FN-70 (Corhart X-317) tested with seed but no ash for 30 hrs. and cycled between 1800°-1600°K. The depth of penetration here is ∿.2 mm. Elemental maps gave results much the same as seen before for the two previously discussed specimens, A Mg deficient layer which contained more Si and K than the bulk. There was some Fe present in the spectra taken from the layer but not as much as was present in the spectra of FN-65. Since there was no ash in this run, it is suggested that Fe must have come from the Mg-Cr bricks used to line the test channel. Elements found in the layer were again Si, K, Ca, Cr, Fe, Mg, and Al.

Virgin X-317 was also examined. Maps and x-ray spectra were taken of the specimen. The results showed that the microstructure of the virgin material was identical to that of the bulk of the tested material. Grains of MgO were located and identified which were much the same as shown in Fig.28a. X-ray spectra showed the presence of Mg, Al, and Ca. Thus, the Ca present in the tested materials was present in the virgin material and not necessarily a result of the testing.

Fig. 26. 100X secondary electron micrograph of Corhart X-317 specimen (FN-27) showing the depth of the reacted layer.

Fig.27a. 500X secondary electron micrograph taken in the polished surface of the reacted layer of FN-27.

Fig.27b. Al area map of the same area.

Fig.27c. Ca area map of the same area.

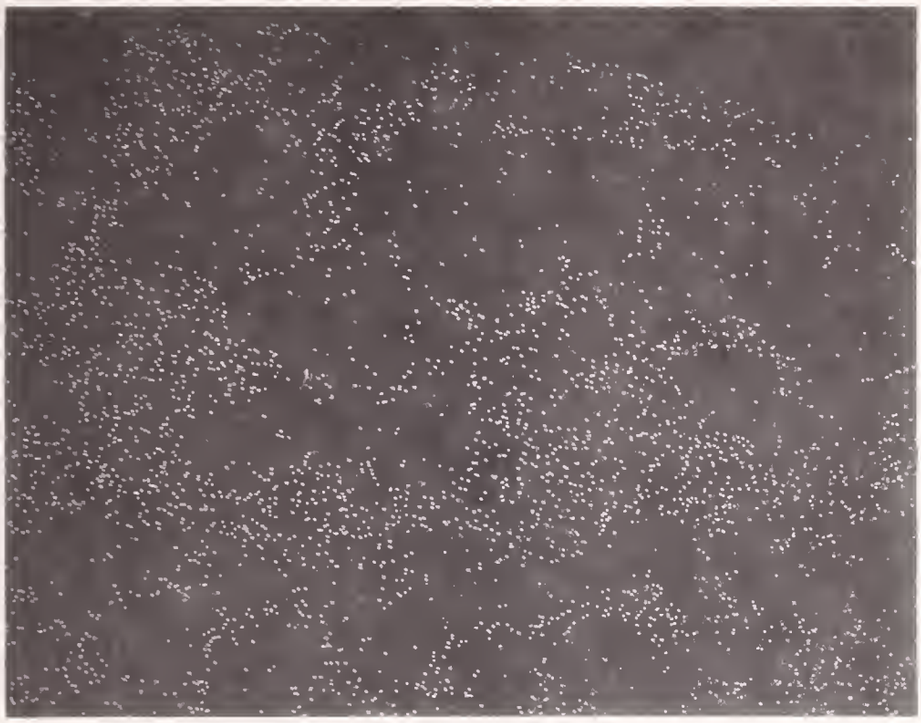

Fig. 27d. Si area map of the same area.

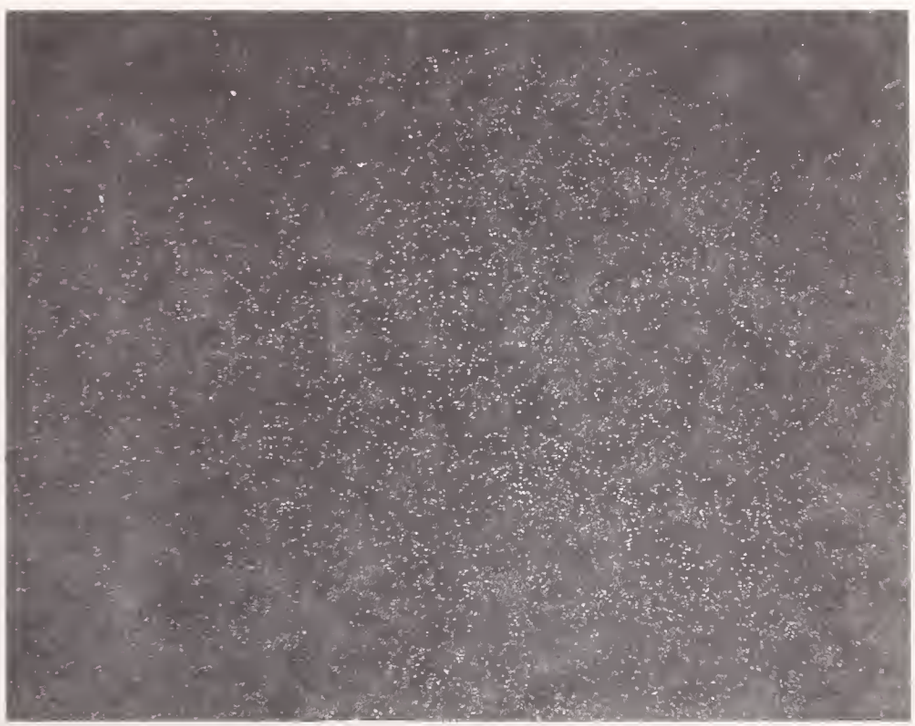

Fig. 27e. Mg area map of the same area.

Fig.28a. 500X backscattered micrograph taken in the bulk of FN-27 showing grains in the $MgAl_2O_4$ matrix.

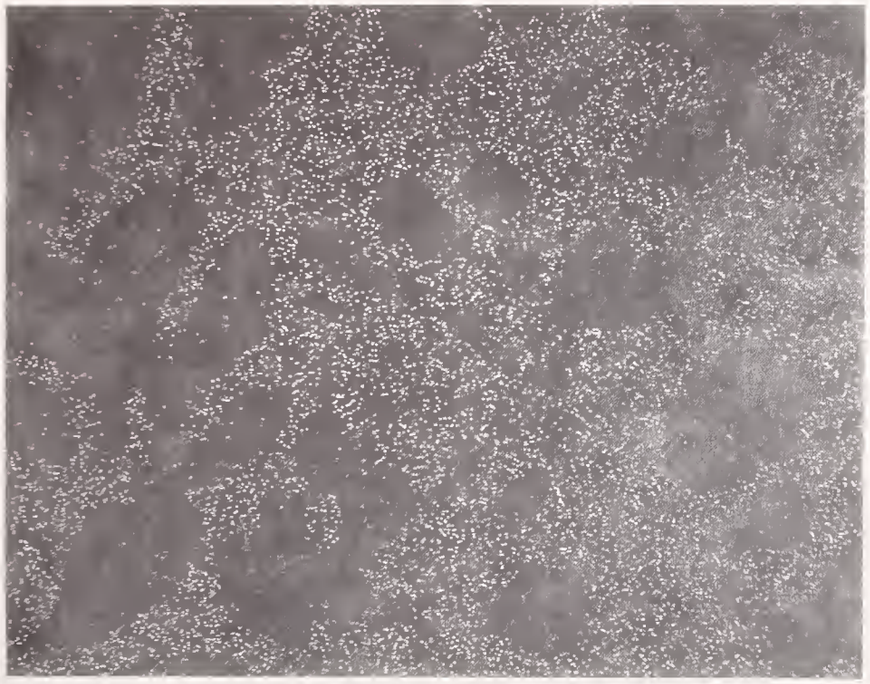

Fig.28b. Al area map of the same area shown in Fig. 28a.

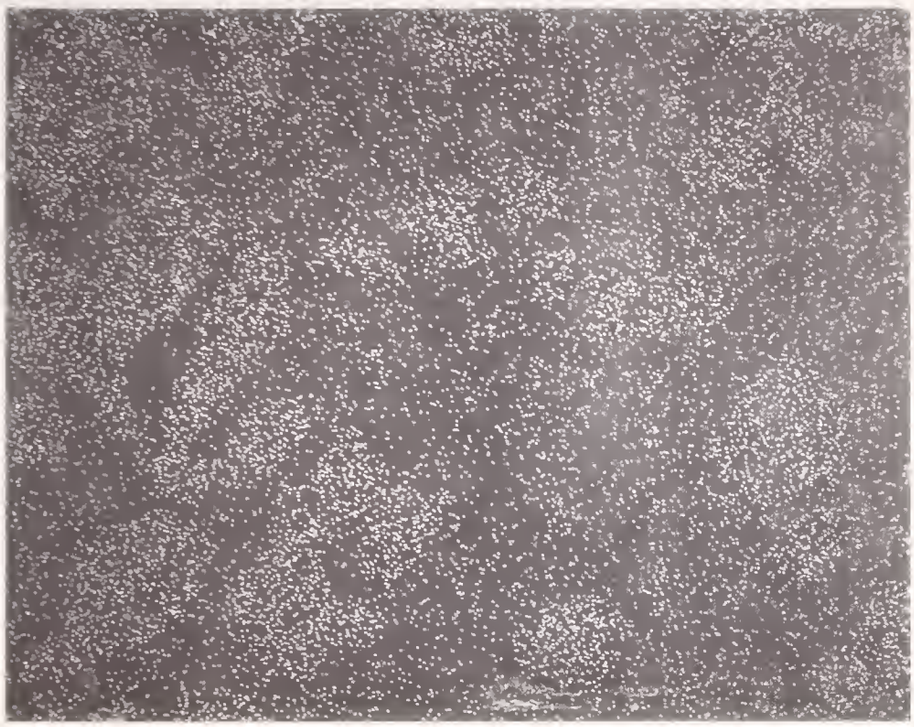

Fig. 28c. Mg area map of the same area shown in Fig. 28a.

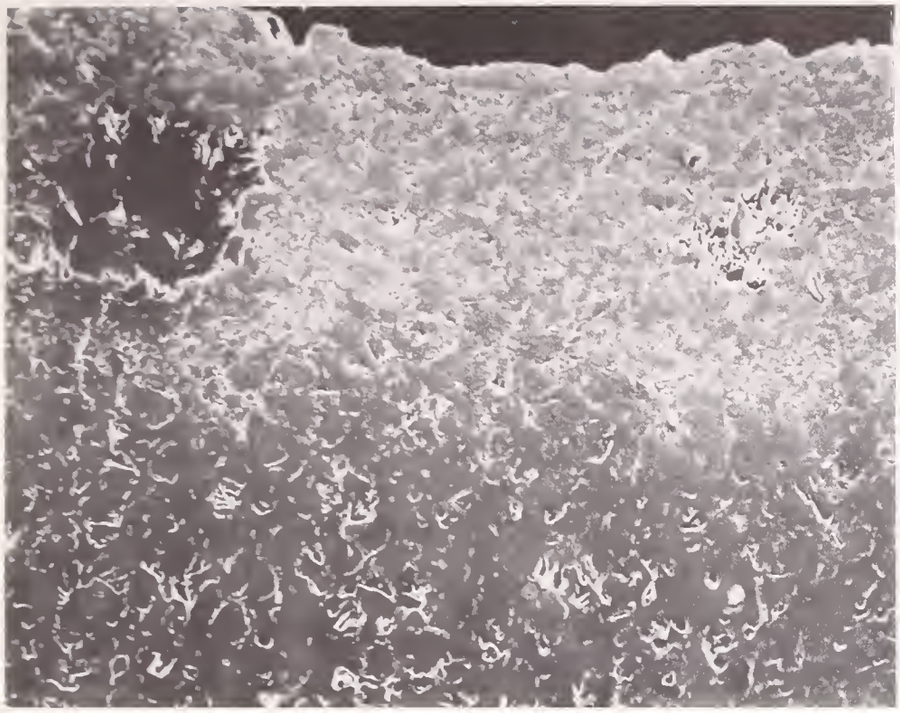

Fig. 29a. 100X secondary electron micrograph of the reacted layer of FN-65.

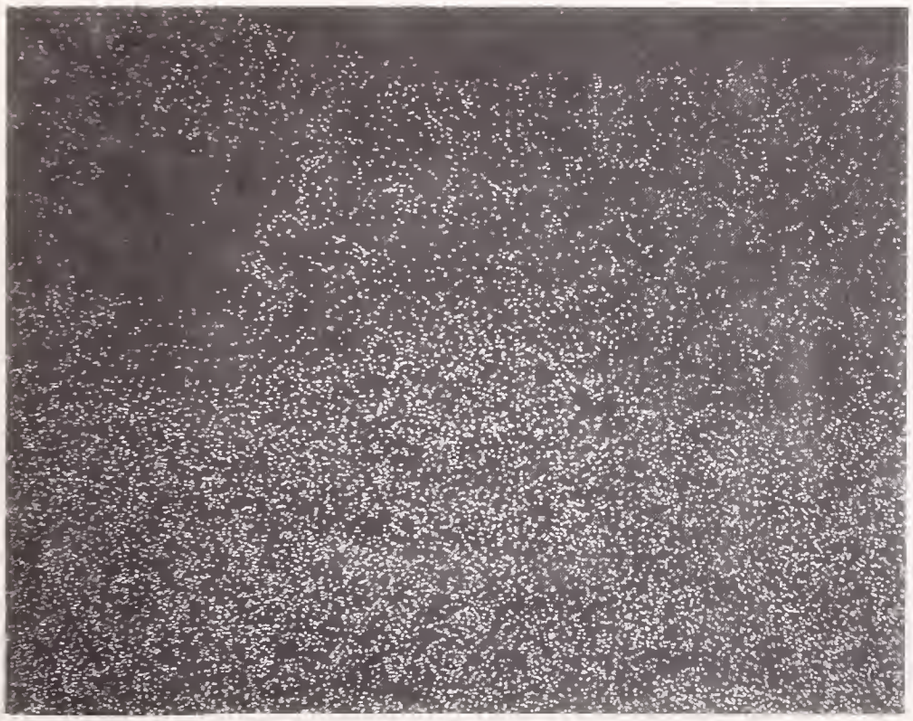

Fig.29b. Mg area map of the same area as in Fig. 29a.

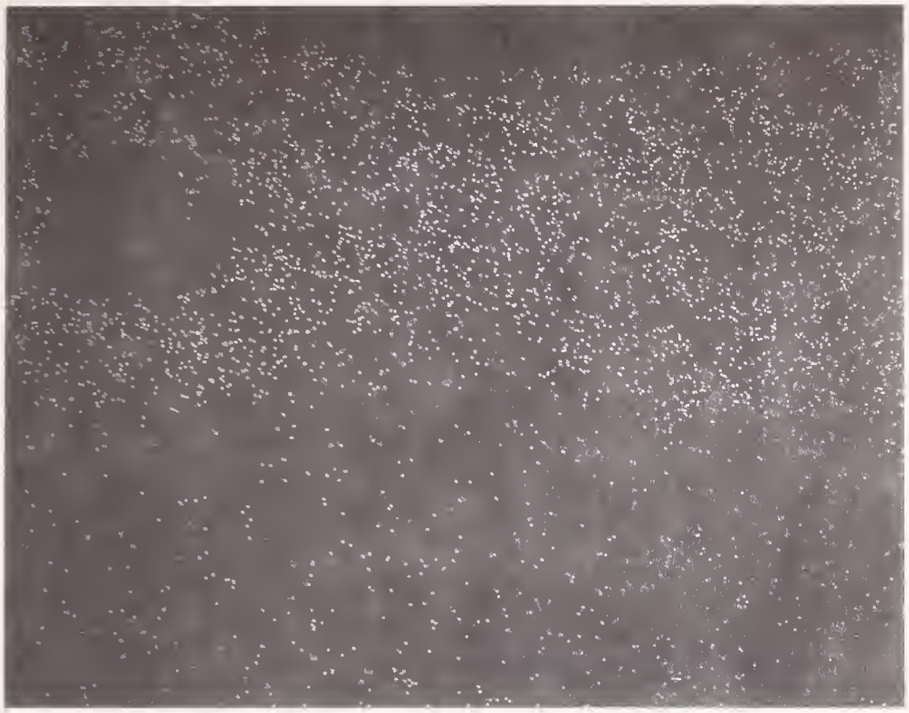

Fig. 29c. Al area map of the same area as in Fig. 29a.

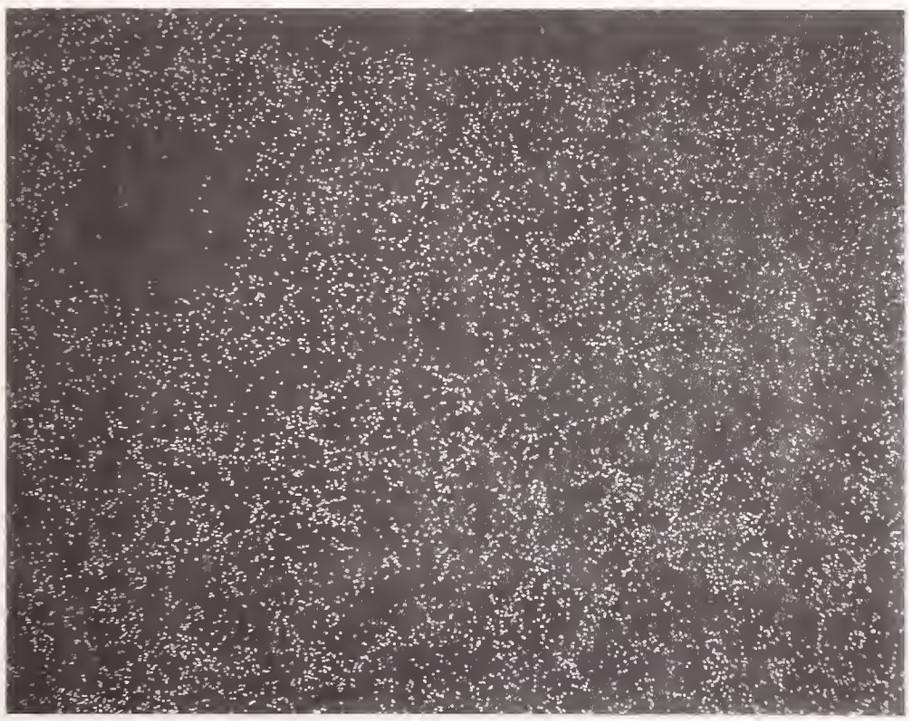

Fig. 29d. Si area map of the same area as in Fig. 29a.

Fig. 30. 200X secondary electron micrograph of the reacted layer of FN-70.

Task L. ASSESSMENT OF STEAM PLANT COMPONENTS (J. R. Cuthill)

This is the 5th quarterly progress report since the initiation of Task L. The "Baseline Plant System Design Description" (1) became available at the beginning of the quarter. Figure 31 is a redrawn block diagram of the system from the combustor through the steam reheater, giving the flue gas temperature at each station and the specified steam temperature and pressure in the steam superheater and reheater. It will be noted that the flue gas temperature is higher in the steam superheater and reheater than in the previous STD calculation, Fig. 32 Another, and possibly more significant difference is in the composition of the flue gas through the steam superheater and reheater, between the previous STD calculation and the Baseline Plant Calculation. The potassium seed going through the superheater and reheater is predominantly K_2CO_3 and K_2SO_4 approximately in the ratio of 2:1 in the previous STD calculation, but is predominantly in the form of sulfate in the Baseline Plant calculation. The latter situation may be a step in the right direction from the point of view of hot-corrosion attack judging from a remark by Stringer in a review paper (2) that an acceleration of oxidation had been observed in a salt-coated test when Na_2CO_3 was substituted for Na_2SO_4.

Hot-corrosion Attack. If the mechanism of hot corrosion attack follows the pattern in marine gas turbines involving sodium compounds, the severity of the K_2SO_4 attack will depend strongly on the amount of KCl present, which fortunately is small but not insignificant, about 1% of the amount of K_2SO_4 present. The effect of the chloride ion content will be discussed in more detail later.

In the Baseline Plant Design, 304H stainless steel [ASTM Spec. A(213) 304H], and 2-1/4 Cr - 1 Mo low alloy steel [ASTM Spec. A(213)T22] (3), is designated for the steam superheater and reheater coils respectively. In view of these steels being specified for the superheater and reheater units it would seem particularly pertinent to summarize the hot corrosion data on these alloys.

Croloy 2-1/4 which complies with SA(213)T22, was included in the simulated MHD corrosion test (4) by the Bureau of Mines at Bruceton (now PERC). (4). The Croloy 2-1/4 was attacked at a wall temperature of 800 °F and a gas temperature of only 1800 °F. They concluded that Croloy 2-1/4 could fulfill "short-term" use at these conditions.

An equivalent steel was included in the simulated MHD hot corrosion test conducted in the Central Electricity Research Laboratories, England. (5) They concluded that 2-1/4 Cr, 1 Mo could be used up to 630 K (675 °F). Note (Fig. 31) that the wall temperature would probably be in this vicinity. An 18 Cr-12 Ni, 1 Nb stainless steel was included in the test program. It showed severe pitting above 725 K rendering it unsafe to use above this temperature. Unfortunately, an 18-8 was not included in the program. Both the PERC and CERL studies are summarized in the ECAS, materials section, (6) but the hot corrosion aspect does not seem to have been taken into account (p. 3-208) in Table 3.10, in which the 304 stainless steel and the 2-1/4 Cr, 1 Mo steel is recommended for the superheater and reheater, respectively.

On the basis of the data available, the 2-1/4 Cr, 1 Mo low alloy steel would not appear to be a viable choice for the reheater, and probably neither is the 304H stainless steel in the case of the superheater unit. Of course, it is understood that such a plant will not be built for a number of years. During the intervening time a continuous reappraisal should be made of the materials selected for the respective components as successively better data becomes available on the actual service conditions to be encountered. For instance, the amount of KCl present with the sulfate appears to be particularly critical.

Schultz and Halsiger (7) discuss results from two different INCO research laboratories using the same "crucible" hot corrosion screening test in their alloy development programs except one used a 10% NaCl-90% Na_2SO_4 molten salt bath and the other used a 25-75% mixture. The latter was much more severe as will be seen by comparing the corrosion rates of IN-738 and UDIMET-500 in Fig. 33 with those in Fig. 34. However, even more spectacular, was the finding that hot corrosion could not be induced in IN-713C in any reasonable length of time when the NaCl was omitted entirely. Also, Stringer (2) warns against increasing the chloride ion content to accelerate corrosion attack because the hot corrosion dependence on chloride concentration has not been established making extrapolation difficult.

For this reason, experimental data on the hot corrosion attack under the specific anticipated service condition needs to be obtained. A test rig that duplicates as nearly as possible the service conditions is unquestionably the straight forward approach for obtaining meaningful data. However, because such tests are expensive and time consuming, in the gas turbine case as well as the MHD case, there have been a number of types of "crucible" tests exploited to try to obtain meaningful correlations with actual service. Schultz and Halsiger (7) have recently described a version called the Salt Shower Test being used at the INCO European Research and Development Center in Birmingham, England. In this test the specimen is mounted on a slowly rotating spindle while maintained at 900 °C or other chosen temperatures in still air. The salt mixture, in the form of dry powder (8), is "showered" down on the specimen either continuously or for 5 minutes every hour. [Fig.35(9)]. This dry powder melts when it hits the hot specimen, running down over it and coating it. In addition to its simplicity and flexibility, this test is reported to overcome the shortcomings of an immersion test in molten salt (which they used previously)in that it will reliably cover cobalt base, as well as nickel base alloys over a wide range of chromium content and a wide spread in resistance to hot corrosion attack.

The compositions of the three wrought alloys showing the exceptional low weight loss in Fig. 34 , i.e., M313, IN-587, and IN-597, (IN-939 is a cast alloy) are given in Table 1. IN-597 is reported to be comparable in strength properties with wrought Udimet-500. Some pertinent mechanical properties of Udimet-500 (10) are tabulated in Table 2.

Future Plans

The immediate emphasis will be on summarizing the hot corrosion data, particularly potassium compounds such as, K_2SO_4, K_2CO_3, KCl and KOH, on the structural alloys being considered. While there is a wealth of data on the hot corrosion attack by sodium compounds, from the marine gas turbine literature, there is comparatively little on potassium compounds but not insignificant. This data on attack by potassium compounds will be summarized.

Another compilation that appears worthwhile is a listing of alloys, considered for heat exchanger tubes, in the order of their resistance to hot-corrosion attack. This ranking will, of necessity, have to be largely on the basis of the marine gas turbine work, because of the limitations on the availability of data.

References

1. Baseline Plant System Design Description, June 30, 1976, by Gilbert Associates and STD Research Corp.

2. John Stringer, Hot Corrosion in Gas Turbine, pp. 79-101, Corrosion Problems in Energy Conversion and Generation, C. S. Tedmon, Jr., Ed. 1974, the Electrochemical Society, Princeton, NJ.

3. 1976 Annual Book of ASTM STandards, Part 1, American Society for Testing and Materials, Philadelphia, PA.

4. D. Bienstock, R. J. Demski, and R. C. Carey, Corrosion of Heat-Exchange Tubes in a Simulated Coal-Fired MHD System, Trans. of ASME, J. of Engineering for Power, 93, A, #2, pp. 249-256.

5. Open Cycle MHD Power Generation, p. 721, J. B. Heywood and G. J. Womack, eds., Pergamon Press, New York.

6. Energy Conversion Alternative Study, Westinghouse, Phase I, Final Report, Vol. II - Materials Considerations, NASA CR-134941, NTIS, Springfield, VA. 22161

7. J. W. Schultz and W. R. Halsiger, Corrosion Resistant Nickel-Base Alloys for Gas Turbines, Metals Engineering Quarterly, 16, 3, pp. 15-24 (1976).

8. Private Communication.

9. P. L. Norman and J. D. Harston, An Evaluation of Commercial High-Chromium Nickel-base Alloys, Deposition and Corrosion in Gas Turbines, A. B. Hart and A. J. B. Cutler, eds. Applied Science Publishers, Ltd., London, 1972.

10. Aerospace Structure Metals Handbook, Vol. 4, Metal Properties Data Center, Belfar Stulen, Inc., 13919 West Bay Shore Drive, Traverse City, Michigan, 49684.

Table 1. Wrought Alloy Compositions

	Cr	Ni	Co	Al	Ti	Nb	Mo	C
M313	30.0	bal.	-	0.9	1.7	-	-	<.06
IN-587	28.5	bal.	20.0	1.2	2.3	0.7	-	.05
IN-597	24.5	bal.	20.0	1.5	3.0	1.0	1.5	.05
UDIMET-500	19.0	bal.	19.0	3.0	3.0	-	4.2	.07

Table 2. Strength Properties of Wrought UDIMET-500
(all properties are at 1200 °F)

100 hr. rupture strength, ksi.	115
Yield strength, ksi.	130
Tensile strength, ksi.	175
0.1% Creep after 1000 hrs, ksi	60

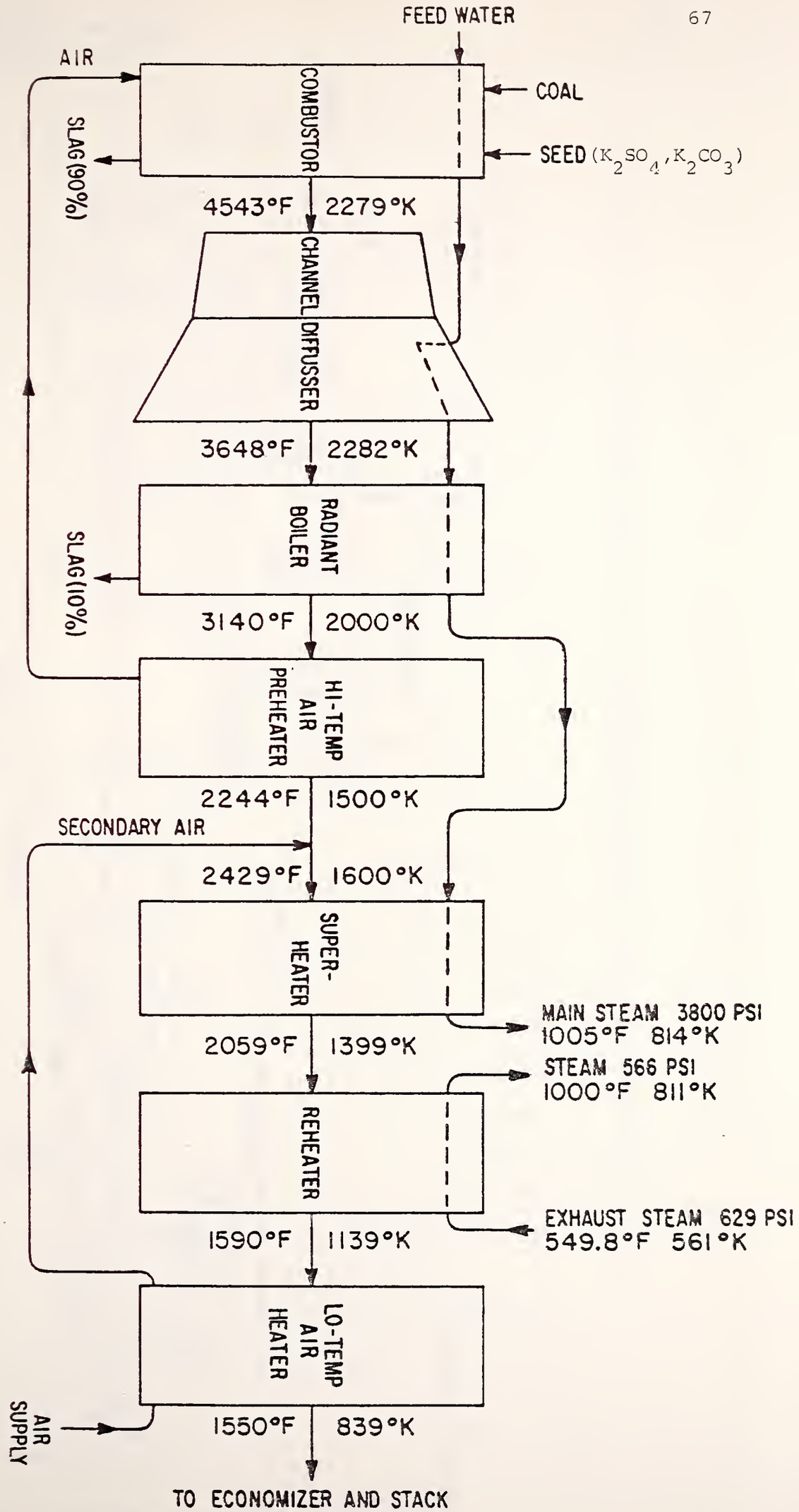

Figure 31. Baseline Reference Design for an Open Cycle MHD Power Plant

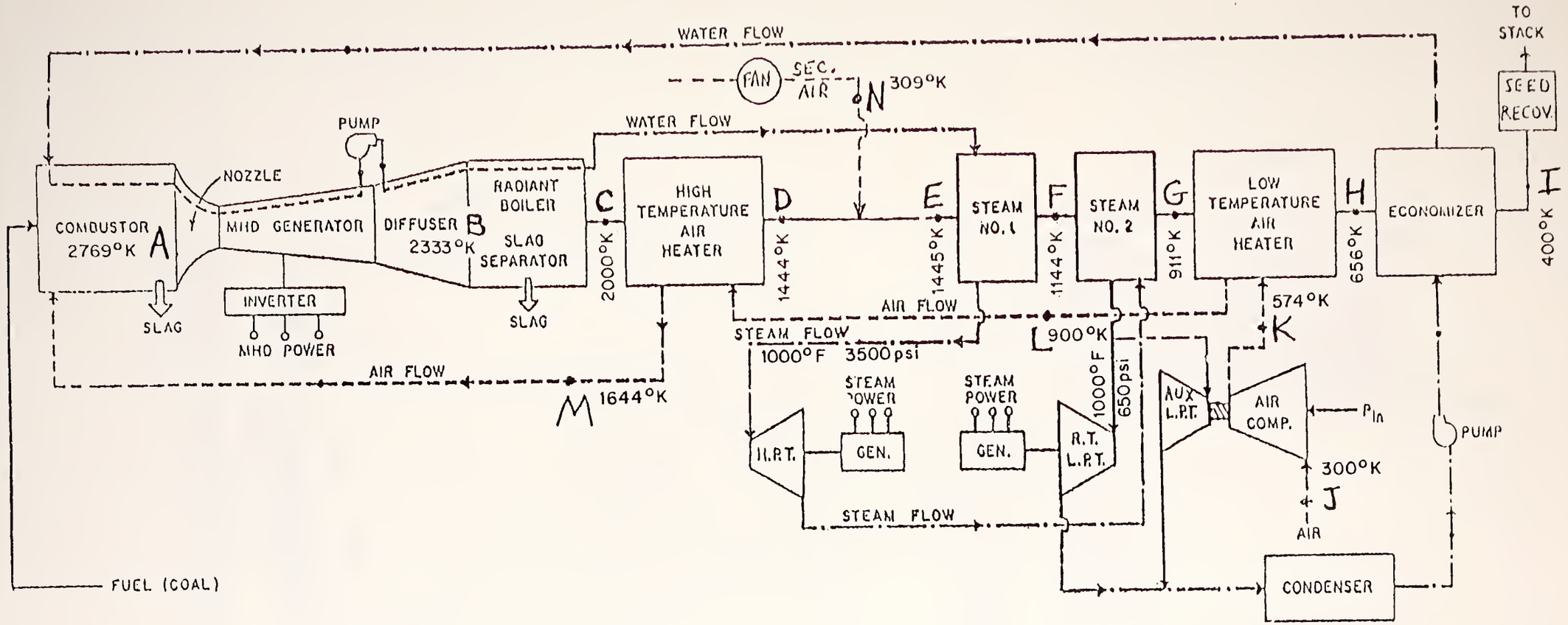

Fig. 32. STD Research Corp. state point temperatures with seed condenser after the steam plant.

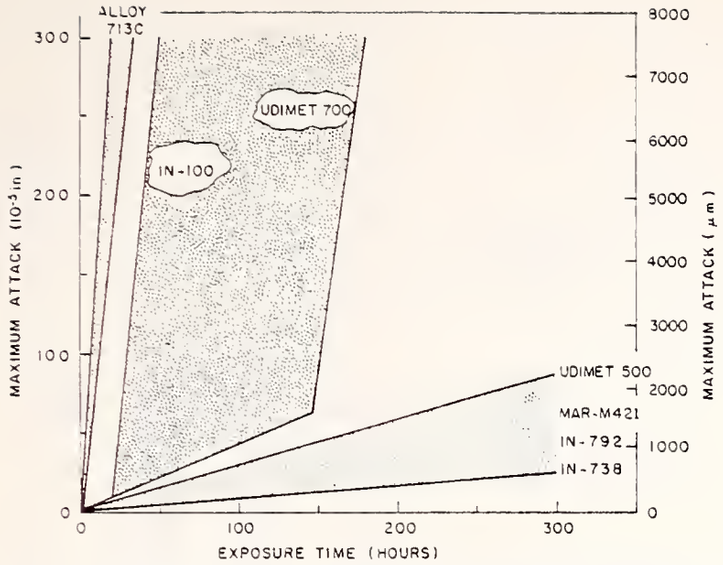

Fig. 33. Comparison of superalloy performance in 90 pct Na_2SO_4-10 pct NaCl crucible test at 927 °C.

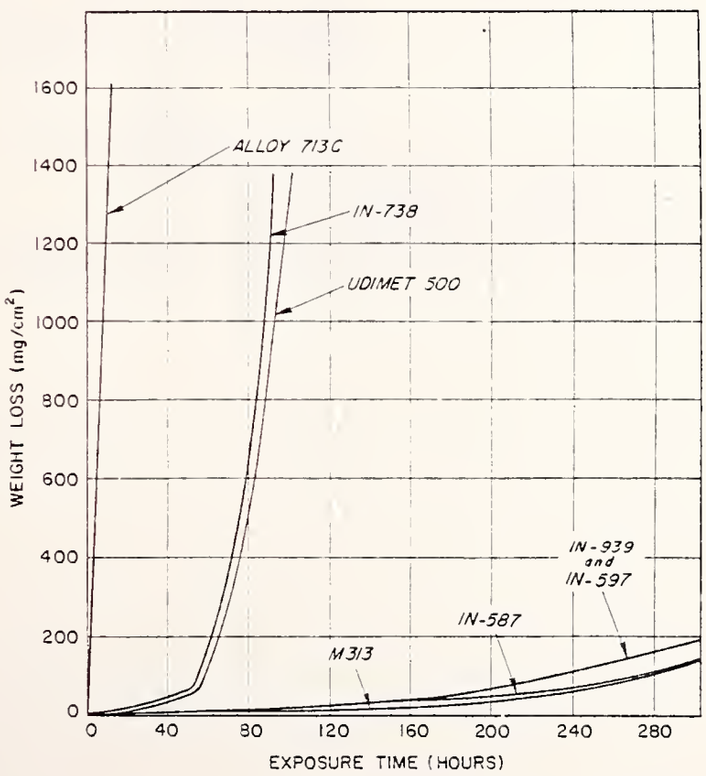

Fig. 34. Comparison of superalloy performance in 75 pct Na_2SO_4-25 pct NaCl salt shower test at 900 °C.

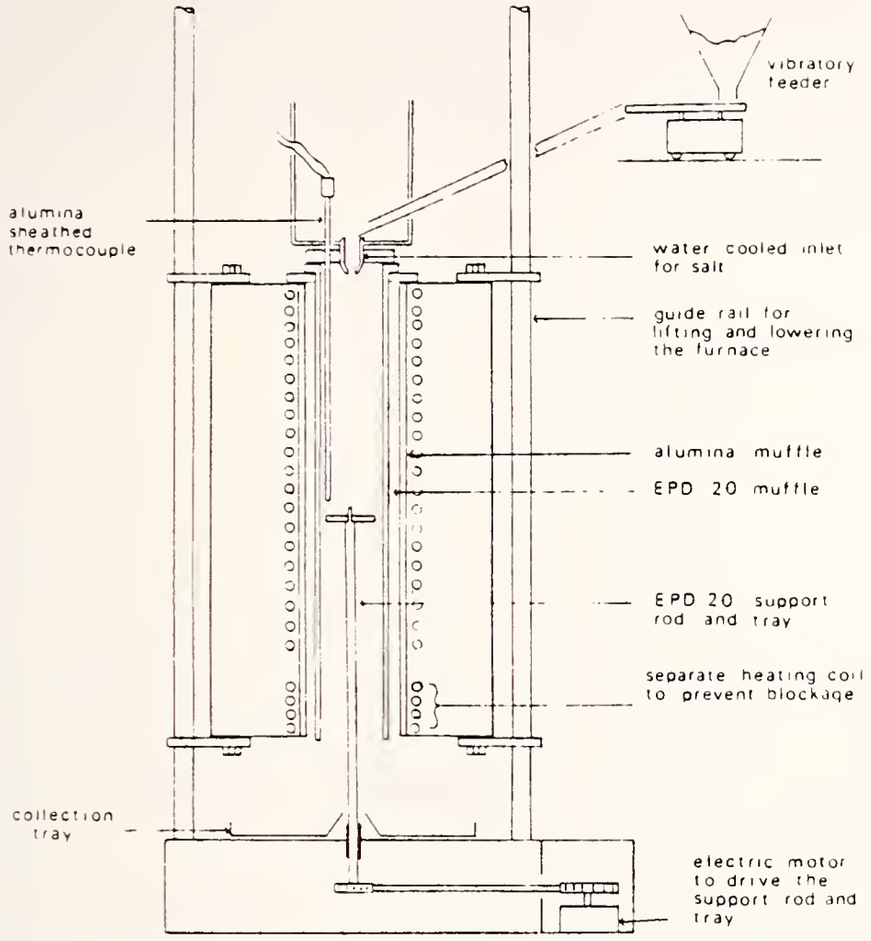

Fig. 35. Schematic diagram showing essential features of the salt shower rig.

76-1151 CANCELLED